JOURNAL OF PETROLOGY | VOLUME 41 | NUMBER 6 | PAGES 809–844 | 2000

# Petrogenesis of Mafic to Felsic Plutonic Rock Associations: the Calc-alkaline Quérigut Complex, French Pyrenees

**MALCOLM P. ROBERTS[1]*, CHRISTIAN PIN[2], JOHN D. CLEMENS[3] AND JEAN-LOUIS PAQUETTE[2]**

[1]DEPARTMENT OF GEOLOGY, UNIVERSITY OF MANCHESTER, MANCHESTER M13 9PL, UK

[2]DÉPARTEMENT DE GÉOLOGIE, UMR 6425 CNRS, UNIVERSITÉ BLAISE PASCAL, 5 RUE KESSLER, 63038 CLERMONT-FERRAND, FRANCE

[3]SCHOOL OF GEOLOGICAL SCIENCES, KINGSTON UNIVERSITY, PENRHYN ROAD, KINGSTON-UPON-THAMES KT1 2EE, UK

**RECEIVED JULY 29, 1998; REVISED TYPESCRIPT ACCEPTED NOVEMBER 23, 1999**

*The Quérigut mafic–felsic rock association comprises two main magma series. The first is felsic comprising a granodiorite–tonalite, a monzogranite and a biotite granite. The second is intermediate to ultramafic, forming small diorite and gabbro intrusions associated with hornblendites and olivine hornblendites. A U–Pb zircon age of 307 ± 2 Ma was obtained from the granodiorite–tonalites. Contact metamorphic minerals in the thermal aureole provide a maximum emplacement pressure of between 260 and 270 MPa. Petrographic characteristics of the mafic and ultramafic rocks suggest crystallization at <300 MPa, demonstrating that mantle-derived magmas ascended to shallow levels in the Pyrenean crust during Variscan times. The ultramafic rocks are the most isotopically primitive components, with textural and geochemical features of cumulates from hydrous basaltic magmas. None of the mafic to ultramafic rocks have depleted mantle isotope signatures, indicating crustal contamination or derivation from enriched mantle. Origins for the diorites include accumulation from granodiorite–tonalite magma, derivatives from mafic magmas, or hybrids. The granitic rocks were formed from broadly Proterozoic meta-igneous crustal protoliths. The isotopic signatures, mineralogy and geochemistry of the granodiorite–tonalites and monzogranites suggest crystallization from different magmas with similar time-integrated Rb/Sr and Sm/Nd isotope ratios, or that the granodiorite–tonalites are cumulates from a granodioritic to monzogranitic parent. The biotite granite differs from the other felsic rocks, representing a separate magma batch. Ages for Quérigut and other Pyrenean granitoids show that post-collisional wrenching in this part of the Variscides was under way by 310 Ma.*

KEY WORDS: *Variscan orogeny; Pyrenees; Quérigut complex; epizonal magmatism; post-thickening; mafic–felsic association*

## INTRODUCTION

Calc-alkaline granitoid rocks are the most abundant constituents of the Earth's continental crust. They are typically associated with post-Archaean orogenic belts and can potentially provide valuable clues to the processes by which the continental crust evolves and differentiates. Here, we present the results of an integrated petrological and geochemical study aimed at constraining the petrogenetic relationships between a wide spectrum of rock types that constitute the Quérigut Massif in the French Pyrenees. This complex is renowned for its spectacular mafic–felsic rock association in which the felsic rocks contain abundant microgranular enclaves interpreted as the products of mingling between coeval granitic and dioritic magmas (e.g. Leterrier, 1972; Marre, 1973; Leterrier & Debon, 1978; Fourcade & Javoy, 1991). Mineral abbreviations recommended by Kretz (1983) are used

*Corresponding author. Present address: Department of Geology, Rhodes University, Grahamstown 6140, South Africa.
e-mail: malc@rock.ru.ac.za

throughout this paper, except for Als, which indicates $Al_2SiO_5$ polymorphs.

A major step in understanding crustal differentiation is to constrain the processes by which granitoid magmas are formed. The broad correspondence of granites to eutectic or minimum melt compositions in the system Qtz–Ab–Or–An–$H_2O$ (e.g. Tuttle & Bowen, 1958; Johannes & Holtz, 1996) suggests that they formed either by fractional crystallization from more mafic parent magmas or by partial melting of pre-existing crustal rocks through 'ultrametamorphism' (White & Chappell, 1977). Partial melting experiments have shown that granitoid magmas can be produced from a wide range of common crustal rocks at geologically realistic temperatures and pressures [see review given by Johannes & Holtz (1996)]. The reactions responsible involve either fluid-absent or fluid-present partial melting during high-grade metamorphism. The geochemistry and mineralogy of the resulting granitic rocks reflect not only the kinds of protoliths from which they were derived, but also the dynamic conditions under which the magmas were formed, evolved and eventually solidified.

Studies of the thermal conditions prevailing in various tectonic settings (Weber & Behr, 1983; England & Thompson, 1984; Wickham & Oxburgh, 1985, 1987; Sandiford & Powell, 1986) provide constraints on the kinds of crustal processes that may be responsible for the formation of granitoid magmas. Thermal conditions arising through crustal thickening will not usually promote widespread magma generation by fluid-absent melting. At these temperatures, the resulting magmas are commonly $H_2O$-rich, low-temperature, near-minimum melts that usually crystallize as migmatites in the middle crust as a result of low thermal energy (Clemens, 1984; Clemens & Mawer, 1992). Clemens & Droop (1998) have provided a detailed analysis of the effects of various *P–T–t* paths, melting reactions and degree of crystal–liquid segregation on granitic melt behaviour.

Calc-alkaline silicic magmas with sufficient thermal and buoyant energy to ascend to the upper crust require extreme thermal conditions for their formation. The reactions involved produce hot, water-undersaturated melts in equilibrium with mafic, refractory granulite residues by fluid-absent breakdown. Such thermal extremes are generally visualized as occurring in the deep crust and require heat input through under- or intraplating of mantle-derived basaltic magmas (e.g. Clemens, 1990; Vielzeuf *et al.*, 1990). This phenomenon may follow crustal thickening events during post-orogenic extension. It should be noted, however, that thickening is not a prerequisite for extension. It can also occur in pull-apart basins along transcurrent faults, or along active or passive continental margins. Nevertheless, a source of heat in the form of mantle-derived magma is thought to be needed for the generation of mobile granitic magmas capable of ascending to the upper crust. Basaltic magmas are an effective means of heat and material transfer into the crust promoting granitoid magma formation (e.g. Huppert & Sparks, 1988). Thus, the close association of rocks with diverse compositions exhibited by calc-alkaline suites would appear to be an intrinsic property of their mode of formation, in the first instance.

Studies of the processes that lead to the genesis of granitoid rock associations with diverse compositions have resulted in the formulation of several other hypotheses. One current model involves magmatic differentiation (e.g. Leake, 1974; Taylor, 1976; Beckinsale *et al.*, 1985; Brophy, 1991), in which magmas evolve towards more felsic compositions by fractional crystallization. This may involve crystal settling (Shaw, 1965), or side-wall crystallization, in which the intrusion becomes more felsic towards the centre (Presnall & Bateman, 1973; Sawka *et al.*, 1990). Intrusion into the upper crust, or eruption, may tap different layers of an underlying, compositionally stratified magma chamber (Hildreth, 1981; Nakada, 1983; Druitt & Bacon, 1989). Magmas may change their compositions by assimilating country rocks or stoped blocks (e.g. Hall, 1966*a*; Hamilton & Myers, 1967; Barker *et al.*, 1975). Variable degrees of partial melting (fractional melting) in the source area (e.g. Hall, 1966*b*; Tepper *et al.*, 1993) may also produce comagmatic suites of contrasting compositions. With rising temperature above the solidus, magmas produced from crustal protoliths shift from granitic to granodioritic in composition (e.g. Robertson & Wyllie, 1971).

Other models include the partial melting of different protoliths in a heterogeneous source region (e.g. Michard-Vitrac *et al.*, 1980; Silver & Chappell, 1988), hybridization between mantle-derived and crustal magmas (e.g. Leterrier, 1972; DePaolo, 1981*a*; Gribble *et al.*, 1990; DePaolo *et al.*,1992) and restite unmixing (White & Chappell, 1977; Wyborn & Chappell, 1986; Chappell *et al.*, 1987; Chappell, 1996). In support of the restite model, Wyllie (1977) suggested that some tonalites may have formed as crystal–liquid mushes. However, although there is much experimental evidence to suggest that these 'non-minimum' liquids contained crystals, there is no reason to assume that their crystals are necessarily restitic in origin (Wall *et al.*, 1987). An alternative view would be that tonalites are accumulations of magmatic crystals from granodioritic to monzogranitic magmas.

Diverse processes, combined with heterogeneous sources, can make mineralogical, geochemical and isotopic data very difficult to interpret, leading to the formulation of misleading or non-unique tectonic models, as well as spurious petrogenetic histories. Consequently, studies of these rocks should integrate several techniques to increase confidence in any resulting model (Clarke, 1992). Using such an approach, we attempt to constrain relationships between the various rocks that form one of

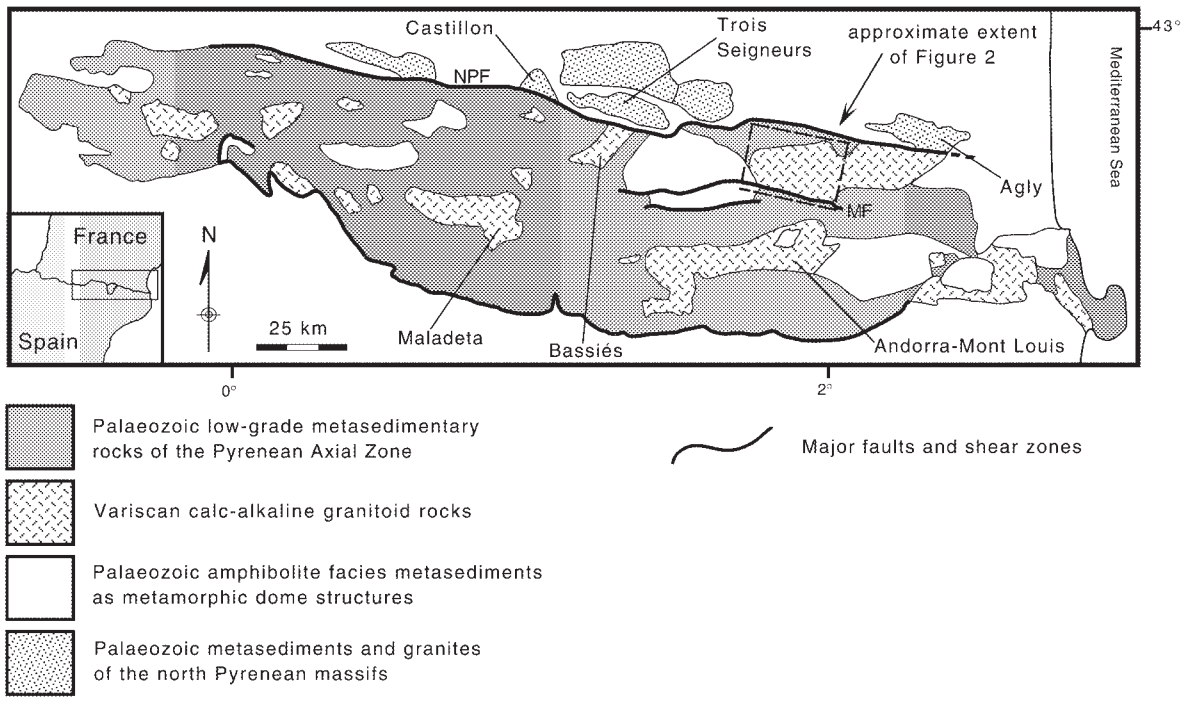


**Fig. 1.** Simplified geological sketch map of the Pyrenean Axial Zone. Modified after Van den Eeckhout & Zwart (1988). MF, Mérens fault.

the world's most well-known and varied calc-alkaline mafic–felsic intrusive suites. We emphasize the need for caution in interpreting geochemical and isotopic data, particularly when applied to such rocks.

## GEOLOGICAL SETTING

The Quérigut Massif forms the western segment of the Quérigut–Millas Massif and, in contrast to its eastern counterpart, contains a wide range of rock types. It is one of several late Variscan calc-alkaline granitoid complexes within the Axial Zone of the Pyrenees, uplifted and exposed as a result of collision between the European and Iberian plates during the late Cretaceous and Eocene. A simplified geological map showing the location of the Massif in the Pyrenean chain is shown in Fig. 1. The Massif (Fig. 2) is surrounded by a narrow contact metamorphic aureole, ~200 m wide, developed in Palaeozoic dolomites and pelites (Leterrier, 1972). These have been metamorphosed into Grs–Di–Ves-bearing skarns and And–Kfs–Ms-bearing metapelites during deformation and intrusion (Aparicio, 1975, 1977). The Massif has been partly truncated in the south by post-intrusion movements along the Mérens fault during Cenozoic tectonism (McCaig & Miller, 1986; Soula *et al.*, 1986).

Previous work has shown that the Massif can be usefully divided into four igneous units (Leterrier, 1972; Marre, 1973). The first is a granodiorite–tonalite unit that forms the southern margin of the Massif and hosts many large metasedimentary xenoliths (dominantly the Grs + Di + Ves-bearing skarns that correlate with the Devonian carbonate unit that crops out along the northern margins of the Massif). Roof pendants within the intrusion represent relicts of a southward-verging thrust sheet that was deformed and metamorphosed during intrusion of the Massif (Raymond & Marre, 1988). The second unit is a monzogranite that forms the bulk of the complex. Contacts between the granodiorite–tonalite unit and the monzogranite appear to be gradational, occurring over a distance of <10 m. The third unit is a central biotite granite, which has sharp contacts against and is entirely surrounded by the monzogranite. Remapping of parts of the Massif as part of this study has shown that the biotite granite unit is smaller than previously thought (cf. Leterrier, 1972). The fourth unit constitutes a number of diorite intrusions, typically decametres to hectometres across, together with subordinate volumes of hornblende gabbro, ultramafic hornblendite and olivine hornblendite. These intermediate to ultramafic masses are mostly associated with the granodiorite–tonalite unit. Previously, the diorites were referred to as 'gabbro–diorite' and the hornblende gabbro as 'gabbronorite' (Leterrier, 1972; Fourcade & Allègre, 1981; Ben Othman *et al.*, 1984; Fourcade & Javoy, 1991). Leterrier (1972) suggested that the ultramafic rocks, which he referred to as 'cortlandtites' (hornblende peridotites; Williams, 1886) represent cumulates. There are also some small, late aplite dykes

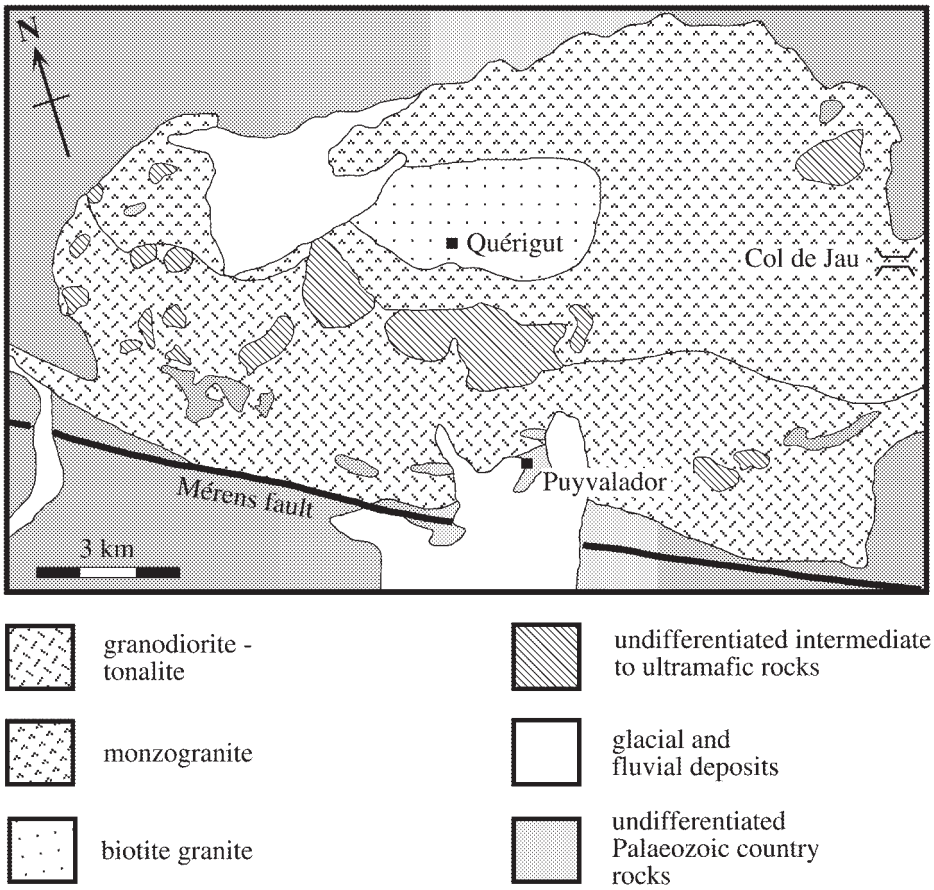


**Fig. 2.** Simplified geological sketch map of the Quérigut Massif. Modified after Leterrier (1972).

cross-cutting the main granitoids, but these are not considered further.

Several hypotheses have been proposed to explain the Quérigut mafic–felsic association. These include fractional crystallization of a single mafic magma, the simultaneous fractional crystallization of mafic and felsic magmas (Marre, 1970, 1973; Pons, 1970) and mixing between mafic and felsic magmas (Leterrier, 1972).

Other models considered include the partial melting of 'wet' continental crust of unspecified composition by mafic magma (Fourcade & Allègre, 1981) and the intrusion of several compositionally distinct, petrogenetically unrelated intrusions (Fourcade & Allègre, 1981; Bickle *et al.*, 1988). The isotopic signatures of the Quérigut granitoids, and other similar contemporaneous intrusive and volcanic rocks in the Pyrenees, highlight the role of reworking of dominantly crustal materials in their genesis (Vitrac-Michard & Allègre, 1975; Michard-Vitrac *et al.*, 1980; Ben Othman *et al.*, 1984; Bickle *et al.*, 1988; Majoor, 1988; Briqueu & Innocent, 1993; Gilbert *et al.*, 1994). Importantly, Leterrier (1972) drew attention to the great complexity of the Quérigut rocks and pointed out that formation of the Massif is unlikely to be due to a single magmatic process. Ben Othman *et al.* (1984) considered assimilation–fractional crystallization (AFC) processes involving mantle-derived mafic magma, coupled with variable degrees of anatexis of gneissic basement. Detailed modelling of the AFC process has been attempted (Roberts & Clemens, 1995, 1997), and has been shown to produce results inconsistent with many aspects of the geochemistry of the rocks despite satisfaction of the isotope systematics. On this basis, AFC does not appear to be an acceptable model for producing the geochemical and isotopic variation among the members of the Quérigut suite.

## PETROLOGY AND MINERAL CHEMISTRY

Table 1 summarizes the major textural and mineralogical features of the various rock types of the Massif. Amphibole end-member compositions (Table 2) were determined with the EMP-AMPH program (Mogessie *et al.*, 1990),

*Table 1: Mineralogical and petrological characteristics of the Quérigut rocks*

| | Olivine hornblendite and hornblendite | Hornblende gabbro | Diorite |
|---|---|---|---|
| Overall texture: | Coarse-grained, poikilitic (Ol hornblendite) | Coarse-grained, sub-ophitic | Medium-grained, euhedral to subhedral granular; Pl-phyric in some cases |
| *Constituent minerals* | | | |
| Qtz | none | none | <5 modal % anhedral, interstitial crystals worm-like inclusions in Hbl* |
| Pl | rare, poikilitically enclosed in Hbl; $An_{82-84}$ in Ol hornblendite; absent in hornblendite | cores and inclusions in Hbl $An_{70-90}$; rims $An_{40-60}$ 25–45 modal % | 30–40 modal % cores $An_{70-80}$ rims $An_{45-60}$ |
| Kfs | none | none | very rare anhedral to interstitial crystals |
| Bt | *mg*-no. 80–90 in Ol hornblendite only; absent in hornblendite | 10–25 modal % *mg*-no. 60–70 | 10–30 modal % *mg*-no. 48–60 |
| Amp | 85 modal %; *mg*-no. 75–85 | 30–50 modal % *mg*-no. 70–80 | 30–40 modal % *mg*-no. 50–70 |
| Ol | poikilitically enclosed in Hbl and Bt; $Fo_{68-83}$ | none | none |
| (in Ol hornblendite only) | | | |
| Accessory minerals | Pyr + Spn + Ilm + ss Ttn | Ilm + Pyr + Sp + ss Ttn | Ilm + Pyr + Ep + Zrn + Ap + primary and ss Ttn |
| Other remarks | Cum and Act after Px; Opx and Cpx absent | some acicular Cum and Act after Px; Opx or Cpx absent | Opx or Cpx absent |

which uses the amphibole classification scheme of Leake (1978). Compositions of biotite and amphibole are expressed as molar Mg/(Mg + Fe*). Typical or representative mineral compositions presented in Tables 2 and 3 are those where multiple analyses showed that the composition did not vary significantly. The complete mineral analysis dataset is omitted for brevity, but can be obtained from the first author on request.

## The felsic rocks

The rocks of these units are coarse grained, and consist of variable amounts of plagioclase, quartz, K-feldspar, biotite and hornblende. All rocks show small amounts of late magmatic to sub-solidus deformation (undulose extinction in quartz and minor sub-grain development along quartz–quartz grain boundaries). Intense deformation related to syn-plutonic faulting has led to the complete recrystallization of quartz and rotation of plagioclase crystals. This is restricted to the southern border of the Massif, within some marginal rocks of the granodiorite–tonalite unit.

Compositions of feldspars from the three felsic units are plotted in Fig. 3. In all cases, the plagioclase occurs as euhedral tablets displaying oscillatory zoning where the variation in An content is no more than 15 mol % from core to rim. This may be attributed to local variation in magma chemistry during crystallization caused by coupled diffusion kinetics in the crystal–melt system (Vance, 1962; Ortoleva, 1994). Generally, the An content of plagioclase decreases from the granodiorite–tonalite unit through the monzogranite unit to the biotite granite. Rare, anhedral cores with compositions as calcic as $An_{60-70}$ are present in the granodiorite–tonalite unit. These cores are mostly altered to sericite and/or clinozoisite and epidote.

In the granodiorites and tonalites, quartz is anhedral and occupies the interstices between plagioclase tablets,

*Table 1: continued*

| | Granodiorite–tonalite | Monzogranite | Biotite granite |
|---|---|---|---|
| Overall texture: | Coarse-grained, euhedral to subhedral | Coarse-grained, euhedral to subhedral granular; mostly Kfs-phyric | Coarse-grained, subhedral granular |
| *Constituent minerals* | | | |
| Qtz | 20–45 modal %<br>anhedral, interstitial crystals<br>worm-like inclusions in Hbl* | euhedral crystals up to 6 mm in dia.;<br>30–50 modal % | euhedral crystals and subhedral patches<br>up to 6 mm in dia.; 20–50 modal % |
| Pl | 35–55 modal %<br>euhedral, oscillatory-zoned tablets; $An_{33–55}$ | euhedral crystals; some oscillatory-zoned;<br>$An_{17–47}$; 15–40 modal % | euhedral crystals; some oscillatory-zoned;<br>$An_{14–40}$; 15–30 modal % |
| Kfs | interstitial microcline crystals; 3–15 modal % | mostly phenocrysts ~3 cm long; both Mc and Or (perthite) present (separately and together); 15–45 modal % | Or (perthite); 30–40 modal % |
| Bt | *mg*-no. 40–50<br>moderate pleochroism | 1–15 modal %<br>*mg*-no. 29–43<br>strongly pleochroic | ~5 modal %; *mg*-no. ~25<br>strongly pleochroic |
| Amp | *mg*-no. 41–64<br>eu- to anhedral crystals; some clots | uncommon;<br>*mg*-no. 38–70 | none |
| Ol and Px | none | none | none |
| Accessory minerals | Ilm + Ap + Zrn + ss and primary | All + Ap + Zrn + ss Ttn, Rut and Ep<br>Ttn + ss Rut + All + primary Ep | Ap + Zrn + ss Ttn |
| Other remarks | poorly developed pleochroic haloes around Zrn inclusions in Bt | minor amounts of myrmekite; prominent pleochroic haloes around Zrn inclusions in Bt | minor amounts of myrmekite; very dark (almost black) pleochroic haloes around Zrn inclusions in Bt |

*Textural evidence for previous existence of liquidus Px.
Mineral abbreviations as recommended by Kretz (1983), except Px, pyroxene. ss, sub-solidus; *mg*-number = 100[molar Mg/(Mg + total Fe)].

suggesting late crystallization. In contrast, quartz in the monzogranite and biotite granite units is typically euhedral to subhedral. All the felsic rocks contain K-feldspar, but its proportion and structural state vary. Compositions are shown in Fig. 3. K-feldspar from the monzogranite and biotite granite typically forms phenocrysts or large anhedral patches engulfing quartz and plagioclase euhedra and plates of biotite, whereas in the granodiorite–tonalite unit, it is interstitial. In the monzogranite unit, K-feldspar occurs as both orthoclase and microcline. Orthoclase-bearing monzogranite is restricted to the northern margin of the Quérigut Massif, with the bulk of the unit being characterized by microcline. Orthoclase is the characteristic K-feldspar type in the biotite granite. In all these felsic rock units, inclusion relationships indicate that K-feldspar crystallized relatively late, even though it is able to form phenocrysts (Vernon, 1986).

Amphibole is common among the rocks of the granodiorite–tonalite unit, where it occurs as clots of anhedral crystals and isolated euhedral crystals. It is rare in the monzogranite unit and absent from the biotite granite. Representative analyses are shown in Table 2. The most common type in the granodiorites and tonalites is magnesio-hornblende, although compositions are diverse. Tiny quartz blebs in hornblende crystals are mantled by pale green actinolite or actinolitic hornblende, and some blue–green, more sodic ferro-edenite or edenitic hornblende occurs as narrow fringes to magnesio-hornblende

*Table 2: Representative major element analyses of amphiboles from the Quérigut rocks, recalculated on the basis of 23 oxygen atoms per formula unit*

| | 1 | 2 | 3 | 4 | 5 | 6 | 7 | 8 | 9 | 10 | 11 | 12 | 13 | 14 | 15 | 16 |
|---|---|---|---|---|---|---|---|---|---|---|---|---|---|---|---|---|
| Unit: | gd–ton | gd–ton | gd–ton | gd–ton | gd–ton | monz | monz | diorite | diorite | gabbro | gabbro | Ol hbl. | Ol hbl | hbl | hbl | Ol hbl |
| $SiO_2$ | 45·38 | 51·67 | 48·21 | 47·05 | 46·67 | 45·03 | 43·25 | 48·57 | 52·53 | 43·75 | 48·04 | 45·00 | 45·72 | 44·63 | 51·09 | 55·67 |
| $TiO_2$ | 1·16 | 0·24 | 0·49 | 1·38 | 1·39 | 1·30 | 1·40 | 0·76 | 0·01 | 2·83 | 0·03 | 2·47 | 1·06 | 2·92 | 0·48 | b.d. |
| $Cr_2O_3$ | b.d. | 0·33 | 0·43 | b.d. | b.d. | b.d. | b.d. | 0·06 | 0·18 | 0·18 | 0·03 | 0·33 | 0·84 | 0·45 | 0·37 | b.d. |
| $Al_2O_3$ | 7·68 | 3·27 | 6·03 | 7·83 | 8·49 | 7·97 | 8·85 | 6·18 | 2·31 | 11·54 | 10·60 | 12·01 | 12·17 | 12·05 | 7·28 | 0·90 |
| FeO* | 19·45 | 16·14 | 18·13 | 17·55 | 17·40 | 21·36 | 21·97 | 14·51 | 13·32 | 8·80 | 7·72 | 6·49 | 6·19 | 8·56 | 7·76 | 11·72 |
| MnO | b.d. | b.d. | b.d. | b.d. | 0·25 | 0·30 | b.d. | 0·25 | b.d. | 0·04 | 0·17 | b.d. | b.d. | b.d. | b.d. | b.d. |
| MgO | 9·25 | 12·58 | 10·74 | 10·81 | 10·65 | 8·27 | 7·48 | 12·78 | 14·38 | 15·41 | 17·60 | 17·54 | 17·79 | 15·76 | 19·28 | 30·12 |
| CaO | 11·61 | 12·05 | 11·63 | 11·82 | 12·14 | 11·04 | 11·22 | 12·02 | 12·55 | 11·24 | 10·70 | 11·69 | 11·78 | 11·54 | 10·47 | 0·89 |
| $Na_2O$ | 1·75 | 0·75 | 0·90 | 1·10 | 1·21 | 1·70 | 1·68 | 0·88 | 0·34 | 2·60 | 2·19 | 2·64 | 2·23 | 2·15 | 1·49 | 0·40 |
| $K_2O$ | 0·88 | 0·22 | 0·62 | 0·55 | 0·76 | 0·94 | 0·99 | 0·47 | 0·10 | 0·34 | 0·03 | 0·49 | 0·58 | 0·55 | 0·12 | b.d. |
| Total | 97·16 | 97·25 | 97·18 | 98·09 | 98·96 | 97·91 | 96·84 | 96·48 | 95·72 | 96·73 | 97·11 | 98·66 | 98·36 | 98·61 | 98·34 | 99·70 |
| Si | 6·900 | 7·617 | 7·193 | 6·945 | 6·867 | 6·830 | 6·663 | 7·179 | 7·758 | 6·335 | 6·719 | 6·303 | 6·381 | 6·306 | 7·016 | 7·426 |
| Ti | 0·137 | 0·027 | 0·054 | 0·151 | 0·150 | 0·146 | 0·167 | 0·089 | 0·000 | 0·304 | 0·000 | 0·261 | 0·109 | 0·314 | 0·049 | 0·000 |
| Cr | — | 0·035 | 0·054 | — | — | — | — | 0·009 | 0·018 | 0·017 | 0·000 | 0·034 | 0·092 | 0·051 | 0·041 | 0·000 |
| $Al^{iv}$ | 1·100 | 0·383 | 0·807 | 1·055 | 1·133 | 1·170 | 1·337 | 0·821 | 0·242 | 1·665 | 1·281 | 1·697 | 1·619 | 1·694 | 0·984 | 0·144 |
| $Al^{vi}$ | 0·280 | 0·184 | 0·251 | 0·311 | 0·343 | 0·252 | 0·273 | 0·254 | 0·158 | 0·302 | 0·466 | 0·289 | 0·385 | 0·309 | 0·196 | 0·000 |
| $Fe^{2+}$ | 2·386 | 1·955 | 1·968 | 1·888 | 1·953 | 2·388 | 2·477 | 1·557 | 1·642 | 0·633 | 0·000 | 0·211 | 0·031 | 0·492 | 0·000 | 0·379 |
| $Fe^{3+}$ | 0·090 | 0·038 | 0·292 | 0·276 | 0·186 | 0·320 | 0·354 | 0·238 | 0·000 | 0·429 | 0·899 | 0·546 | 0·690 | 0·518 | 0·891 | 0·927 |
| Mn | — | — | — | — | 0·035 | 0·036 | — | 0·036 | — | 0·009 | 0·017 | — | — | — | — | — |
| Mg | 2·102 | 2·763 | 2·386 | 2·378 | 2·333 | 1·870 | 1·721 | 2·817 | 3·169 | 3·325 | 3·671 | 3·661 | 3·698 | 3·318 | 3·945 | 5·984 |
| Ca | 1·891 | 1·904 | 1·857 | 1·871 | 1·909 | 1·797 | 1·851 | 1·902 | 1·988 | 1·740 | 1·604 | 1·750 | 1·761 | 1·748 | 1·544 | 0·128 |
| Na | 0·512 | 0·213 | 0·260 | 0·310 | 0·345 | 0·502 | 0·500 | 0·249 | 0·098 | 0·731 | 0·596 | 0·715 | 0·603 | 0·586 | 0·396 | 0·104 |
| K | 0·174 | 0·044 | 0·117 | 0·106 | 0·141 | 0·182 | 0·194 | 0·089 | 0·018 | 0·061 | 0·008 | 0·084 | 0·101 | 0·102 | 0·025 | — |
| Sum | 15·572 | 15·163 | 15·239 | 15·291 | 15·395 | 15·494 | 15·537 | 15·240 | 15·091 | 15·551 | 15·261 | 15·551 | 15·470 | 15·438 | 15·087 | 15·092 |
| *mg*-no. | 45·9 | 58·1 | 51·4 | 52·4 | 52·2 | 40·8 | 37·8 | 61·1 | 65·9 | 75·8 | 80·3 | 82·9 | 83·7 | 76·7 | 81·6 | 82·1 |

1, Ferro-edenite fringe to magnesio-hornblende crystal analysis 3; sample QH76. 2, Actinolite aureole to quartz bleb in magnesio-hornblende (after Cpx?); sample QH76. 3, Magnesio-hornblende sub- to euhedral grain with blue fringe (analysis 1); sample QH76. 4, Magnesio-hornblende subhedral crystal from hornblende clot; sample QH29. 5, Magnesio-hornblende euhedral crystal in contact with plagioclase, quartz and biotite; sample QH29. 6, Ferro-hornblende from anhedral ragged clot; sample QH45. 7, Ferro-edenitic hornblende from anhedral ragged clot; sample QH45. 8, Magnesio-hornblende euhedral crystal in groundmass surrounded by plagioclase and biotite; sample QM236. 9, Actinolite aureole to quartz bleb hosted by hornblende analysis 8 (after Cpx?); sample QM236. 10, Titanian magnesio-hastingsitic hornblende brown core to phenocryst; sample QM119. 11, Ferrian magnesio-hornblende rim to phenocryst (core analysis is 10); sample QM119. 12, Titanian magnesio-hastingsitic hornblende brown core analysis from large crystal with poikilitic olivine; sample QUM6. 13, Tschermakitic hornblende rim analysis from large crystal with poikilitic olivine (core analysis is 12); sample QUM6. 14, Titanian tschermakitic hornblende brown core analysis from large crystal; sample QUM5. 15, Ferrian magnesio-hornblende rim analysis from large crystal (core analysis is 14); sample QUM5. 16, Cummingtonite acicular fringe developed around hornblende crystal without poikilitic olivine; sample QUM226. b.d., below detection limit; *mg*-number = 100[molar Mg/(Mg + Fe*)]. FeO*, total Fe as FeO. Fe* = $Fe^{2+}$ + $Fe^{3+}$. OH, F and Cl not analysed. Ol hbl, olivine hornblendite; hbl, hornblendite; gd–ton, granodiorites and tonalites; monz, monzogranites.

crystals. The presence of the tiny anhedral quartz inclusions in the hornblende crystals (see Fig. 4) may be evidence that the hornblende formed through a peritectic reaction involving primary, near-liquidus clinopyroxene. This process may occur in two stages. The first stage, in the presence of melt, would lead to the armouring of the clinopyroxene crystal with a rind of hornblende through a reaction of the form

$$\text{Cpx} + \text{hydrous melt} \rightarrow \text{Hbl}.$$

*Table 3: Representative major element analyses of biotites from the Quérigut rocks, recalculated on the basis of 22 oxygen atoms p.f.u.*

| | 1 | 2 | 3 | 4 | 5 | 6 | 7 | 8 | 9 | 10 | 11 | 12 | 13 | 14 |
|---|---|---|---|---|---|---|---|---|---|---|---|---|---|---|
| Unit: | diorite | diorite | diorite | gabbro | gabbro | gabbro | Ol hbl | Ol hbl | gd–ton | gd–ton | monz | monz | Bt grn | Bt grn |
| $SiO_2$ | 36·64 | 37·64 | 37·74 | 37·95 | 38·30 | 38·20 | 36·82 | 38·75 | 36·01 | 35·59 | 35·71 | 35·57 | 36·00 | 35·96 |
| $TiO_2$ | 2·59 | 1·70 | 1·42 | 0·71 | 1·33 | 1·90 | 0·44 | 0·41 | 2·92 | 2·59 | 4·12 | 3·96 | 2·39 | 2·53 |
| $Cr_2O_3$ | n.a. | n.a. | n.a. | n.a. | 0·29 | 0·22 | 0·33 | n.a. | n.a. | n.a. | n.a. | n.a. | n.a. | n.a. |
| $Al_2O_3$ | 16·07 | 16·93 | 17·14 | 16·86 | 16·51 | 15·80 | 14·56 | 17·72 | 15·83 | 16·18 | 13·86 | 13·74 | 18·77 | 18·29 |
| FeO* | 19·19 | 18·47 | 19·38 | 13·00 | 12·32 | 11·88 | 5·66 | 5·56 | 21·97 | 21·43 | 25·20 | 24·68 | 24·79 | 25·06 |
| MnO | b.d. | b.d. | b.d. | 0·19 | b.d. | b.d. | b.d. | b.d. | b.d. | b.d. | b.d. | b.d. | b.d. | b.d. |
| MgO | 10·57 | 11·52 | 11·35 | 17·66 | 16·00 | 16·30 | 25·93 | 22·59 | 8·70 | 8·89 | 8·41 | 8·39 | 5·02 | 5·14 |
| CaO | 0·22 | b.d. | 0·25 | 0·09 | b.d. | b.d. | b.d. | 0·12 | b.d. | b.d. | b.d. | b.d. | b.d. | 0·14 |
| $Na_2O$ | 0·44 | 0·32 | 0·38 | 0·12 | 0·42 | 0·36 | 0·43 | 1·61 | 0·43 | 0·43 | 0·44 | 0·22 | 0·37 | 0·34 |
| $K_2O$ | 9·36 | 9·67 | 9·63 | 8·33 | 8·84 | 8·84 | 6·56 | 7·61 | 9·45 | 9·37 | 9·15 | 9·14 | 9·50 | 9·68 |
| Total | 95·08 | 96·25 | 97·29 | 94·91 | 94·01 | 93·50 | 90·73 | 94·37 | 95·31 | 94·48 | 96·89 | 95·70 | 96·84 | 97·14 |
| Si | 5·597 | 5·639 | 5·617 | 5·579 | 5·681 | 5·691 | 5·458 | 5·525 | 5·572 | 5·543 | 5·533 | 5·567 | 5·523 | 5·520 |
| Ti | 0·298 | 0·192 | 0·159 | 0·079 | 0·148 | 0·213 | 0·049 | 0·044 | 0·340 | 0·303 | 0·480 | 0·466 | 0·276 | 0·292 |
| Cr | — | — | — | — | 0·034 | 0·026 | 0·039 | — | — | — | — | — | — | — |
| $Al^{iv}$ | 2·403 | 2·361 | 2·383 | 2·421 | 2·319 | 2·309 | 2·542 | 2·475 | 2·428 | 2·457 | 2·467 | 2·433 | 2·477 | 2·480 |
| $Al^{vi}$ | 0·490 | 0·627 | 0·623 | 0·500 | 0·566 | 0·465 | 0·001 | 0·502 | 0·459 | 0·513 | 0·064 | 0·101 | 0·916 | 0·828 |
| $Fe^{2+}$ | 2·451 | 2·314 | 2·412 | 1·598 | 1·528 | 1·480 | 0·702 | 0·663 | 2·843 | 2·791 | 3·265 | 3·230 | 3·180 | 3·216 |
| Mn | — | — | — | 0·024 | — | — | — | — | — | — | — | — | — | — |
| Mg | 2·407 | 2·573 | 2·518 | 3·870 | 3·538 | 3·620 | 5·730 | 4·801 | 2·007 | 2·064 | 1·943 | 1·958 | 1·148 | 1·176 |
| Ca | 0·036 | — | 0·040 | 0·014 | — | — | — | 0·018 | — | — | — | — | — | 0·023 |
| Na | 0·130 | 0·093 | 0·110 | 0·034 | 0·121 | 0·104 | 0·124 | 0·445 | 0·129 | 0·130 | 0·132 | 0·067 | 0·110 | 0·101 |
| K | 1·824 | 1·848 | 1·828 | 1·562 | 1·672 | 1·680 | 1·240 | 1·384 | 1·865 | 1·862 | 1·808 | 1·825 | 1·859 | 1·895 |
| Sum | 15·636 | 15·646 | 15·690 | 15·680 | 15·608 | 15·588 | 15·884 | 15·857 | 15·642 | 15·664 | 15·692 | 15·646 | 15·489 | 15·532 |
| *mg*-no. | 49·5 | 52·6 | 51·1 | 70·8 | 69·8 | 71·0 | 89·1 | 87·9 | 41·4 | 42·5 | 37·3 | 37·7 | 26·5 | 26·8 |

1, Euhedral crystal in contact with hornblende and plagioclase; sample QM50. 2, Anhedral growth in hornblende crystal; sample QM50. 3, Crystal in mafic (hornblende–biotite) clot; sample QM50. 4, Anhedral growth in hornblende crystal; sample QM119. 5, Euhedral blade in hornblende phenocryst; sample QM77. 6, Anhedral growth in hornblende crystal; sample QM77. 7, Anhedral, interstitial crystal poikilitic to olivine; sample QUM6. 8, Anhedral, interstitial crystal poikilitic to olivine and plagioclase; sample QUM226. 9, Prism edge of crystal in mafic (hornblende–biotite–epidote) clot; sample QH76. 10, Euhedral crystal with zircon and apatite inclusions; biotite in contact with plagioclase and quartz; sample QH76. 11, Crystal adjacent to euhedral allanite; sample QH45. 12, Eu- to subhedral crystal with zircon and apatite inclusions; sample QH45. 13, Prism edge of blade-shaped crystal surrounded by plagioclase, quartz and K-feldspar; sample QH89. 14, Prism edge of blade-shaped crystal surrounded by plagioclase, quartz and K-feldspar; sample QH89. Fe analysed as FeO and expressed as $Fe^{2+}$; *mg*-number = 100[molar Mg/(Mg + $Fe^{2+}$)]; $Al^{vi}$ calculated assuming Si + $Al^{iv}$ = 8. OH, F and Cl not analysed. n.a., not analysed; b.d., below detection limit. Bt grn, biotite granite; other rock name abbreviations as in Table 2.

The second stage is similar to the first, although more sluggish, and most probably involves the diffusion of Al and OH ions through the hornblende rind:

$$\mathrm{Cpx} + \mathrm{Al,\ OH} \rightarrow \mathrm{Hbl} + \mathrm{Qtz}.$$

The extra $SiO_2$ from the expiring pyroxene becomes trapped and nucleates as quartz, more or less *in situ* within the modifying crystal lattice during replacement. The mantle of actinolite reflects local enhancement of $a SiO_2$ around the quartz blebs. The rare hornblende crystals found in the monzogranite indicate an origin through alteration of primary clinopyroxene and are extremely ragged in appearance.

Representative analyses of biotite are presented in Table 3. Chemical variation of this mineral between the three felsic units is shown graphically in Fig. 5. Biotite in the monzogranite is more Fe rich than that in the granodiorites and tonalites, whereas that of the biotite granite is more Fe rich than in the other two units, and markedly more aluminous. In the granodiorite–tonalite and monzogranite units, biotite forms individual crystals, clots and anhedral patches inside euhedral to subhedral hornblende crystals. In this third case, contacts between the two minerals are very irregular and suggest a reaction relation, where biotite is probably replacing hornblende in response to increasing $a K_2O$ in the melt during

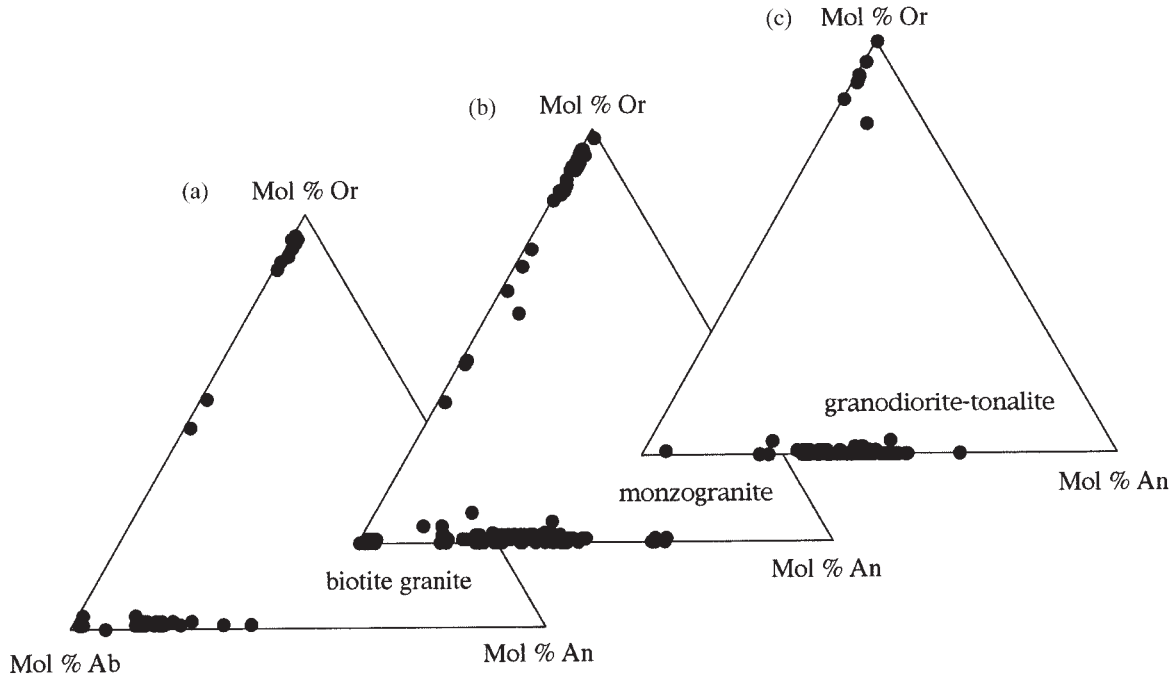


**Fig. 3.** Compositional ranges of plagioclase and K-feldspar analyses from (a) biotite granite, (b) monzogranite and (c) granodiorite–tonalite units.

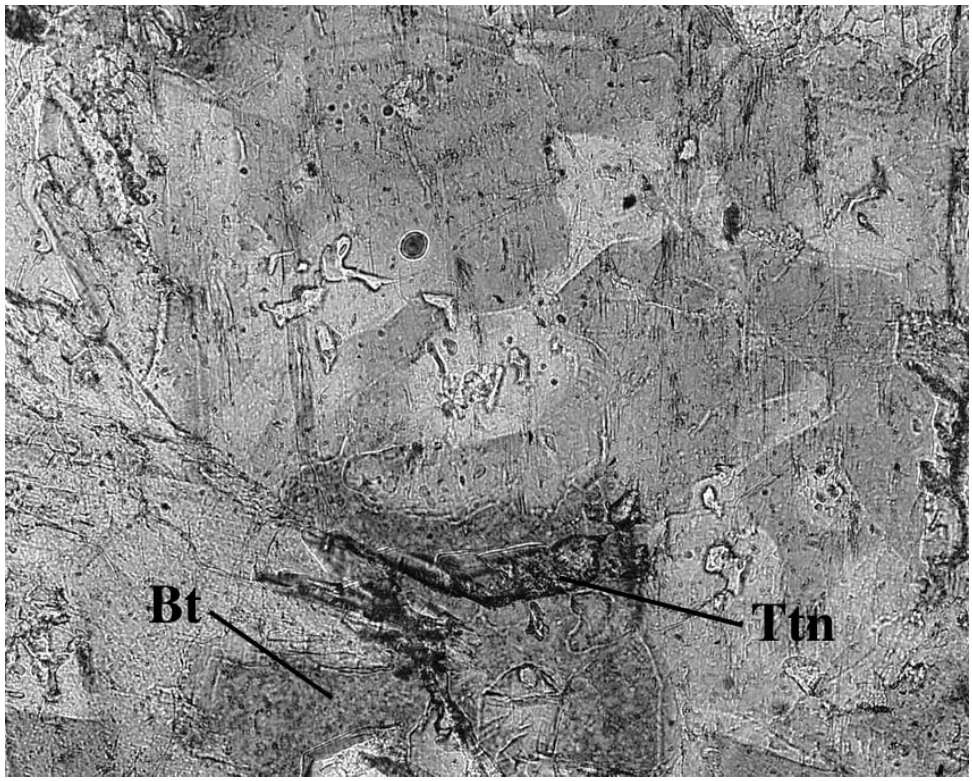


**Fig. 4.** Anhedral, worm-like blebs of quartz surrounded by haloes of actinolite (pale grey) in a subhedral magnesio-hornblende crystal in diorite QM236. [Note incipient replacement of hornblende by biotite (Bt; dark grey), as well as polycrystalline aggregates of titanite (Ttn; high relief), possibly after ilmenite.] Length of field of view is 0·6 mm. Plane-polarized light.

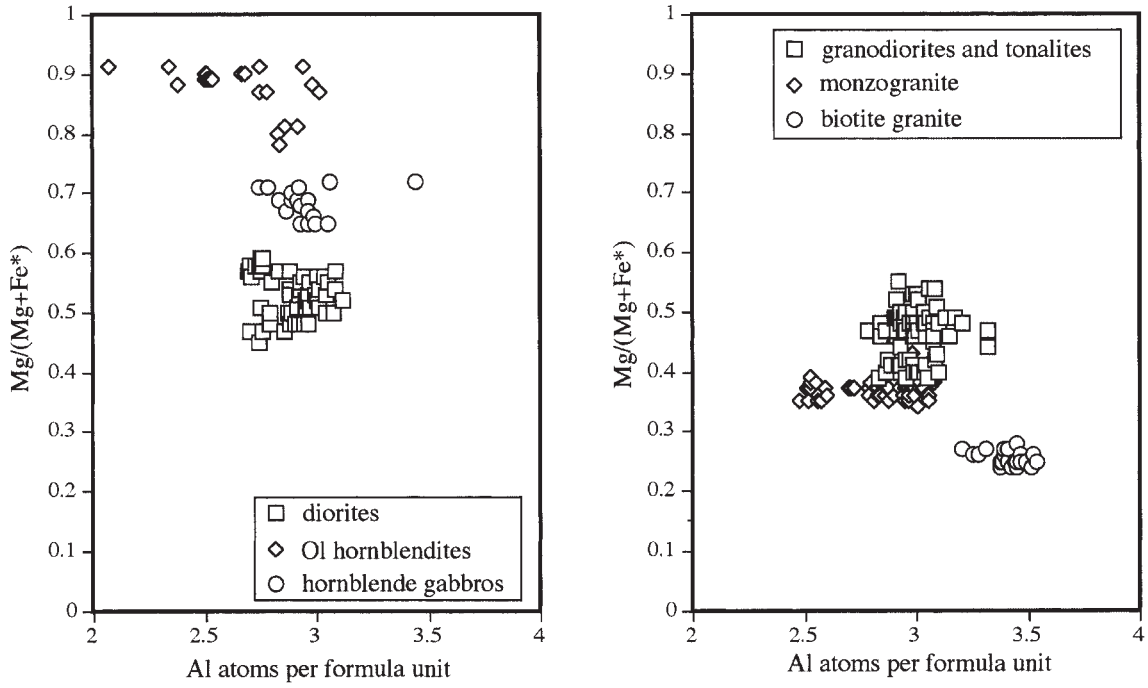


**Fig. 5.** Plots of Al p.f.u. vs Mg/(Mg + Fe*) for biotite compositions from the Quérigut rocks. Fe* is total Fe p.f.u. as FeO.

crystallization. In all cases, the value of Mg/(Mg + Fe*) for the biotite is lower than that of coexisting hornblende.

Epidote occurs not only from the sub-solidus alteration of plagioclase, but also in mafic mineral clots or mantled by biotite. Contacts with biotite are sharp. These textures and mineral associations are considered as evidence for the magmatic origin of this epidote (see Zen & Hammarstrom, 1984). Analysis shows that its composition falls within the range of magmatic epidote [pistacite mole fraction of 0·2–0·3 ( Johnston & Wyllie, 1988); ferric iron contents calculated using the method of Droop (1987)].

## The mafic rocks

The intermediate to ultramafic rocks contain variable amounts of plagioclase, hornblende and biotite, with minor quartz and rare K-feldspar in the diorites. The diorites are medium grained and euhedral to subhedral granular; some samples are plagioclase phyric. The gabbros, hornblendites and olivine hornblendites are coarse grained and consist dominantly of interlocking frameworks of amphibole crystals. The textures of these units are typical for mafic igneous rocks: the gabbros are subophitic, and the olivine hornblendites are poikilitic with hornblende oikocrysts. In contrast to the report of Leterrier (1972), no pyroxene was found in any of the samples collected for this study. The difference between the hornblendites and the olivine hornblendites is the presence of olivine, biotite and rare plagioclase in the latter.

Plagioclase compositions are plotted in Fig. 6. In the olivine hornblendites, calcic plagioclase ($An_{82–84}$) occurs as euhedra enclosed in poikilitic hornblende. In contrast, plagioclase is a major constituent of the hornblende gabbros and diorites, where its compositional distribution is bimodal. This is seen texturally as anhedral calcic ($An_{80–90}$) cores surrounded by euhedral, less calcic, oscillatory-zoned overgrowths of $An_{40–60}$. In the diorites, some of the cores have low-amplitude oscillatory or normal zoning. Unzoned, euhedral plagioclase crystals enclosed by hornblende in the hornblende gabbros have the same compositions as the overgrown cores. Minor amounts of quartz and very rare K-feldspar (microcline) are present in some diorites. Both minerals occur interstitially to the main mineral assemblage, indicating late crystallization. Small anhedral blebs of quartz also occur as inclusions in some hornblende crystals from the hornblende gabbros and diorites, suggesting the former presence of pyroxene.

Amphibole is present in all the intermediate to ultramafic rocks of the Quérigut Massif. Table 2 shows some representative analyses. In these rocks, the dominant amphibole is magnesio-hornblende. Pargasitic, tschermakitic and edenitic hornblende are sometimes present in the ultramafic rocks and in these, and the hornblende gabbros, zoning is also common. Figure 7 shows the CIPW normative quartz and nepheline compositions

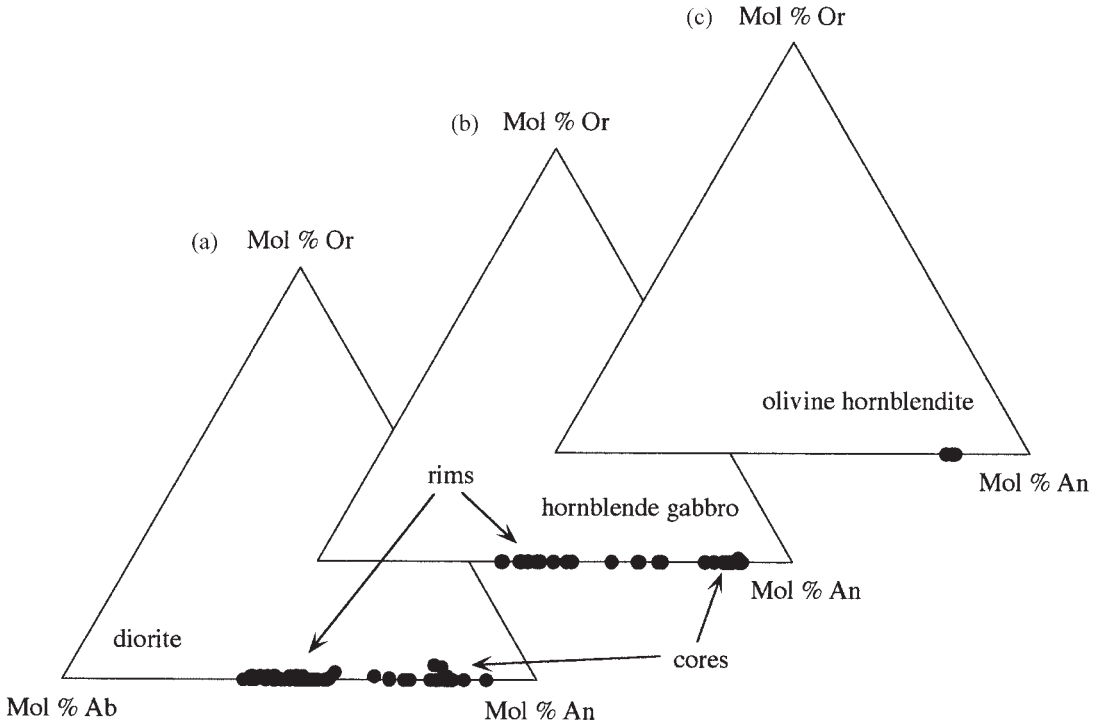


**Fig. 6.** Compositional ranges of plagioclase analyses from (a) diorite, (b) hornblende gabbro and (c) olivine hornblendite.

of amphiboles from the hornblendites and the olivine hornblendites, highlighting the zoning and differences in mineral chemistry between the two rock types. Zoning in the amphiboles of the hornblendites and olivine hornblendites occurs as Ti-rich brown crystal cores with low-Ti green concentric rims or anhedral patches distributed throughout the crystal (which explains the wide range of Ti contents for the cores in Fig. 7). Hornblende cores and rims from the hornblendites are generally more $SiO_2$ rich than those in the olivine hornblendites, which indicates differences in the chemistry of the magmas from which these rocks crystallized (Cawthorn, 1976).

Some rounded Ti-rich hornblendes in the hornblendites are mantled by acicular actinolite, which plots in the $SiO_2$-oversaturated field in Fig. 7 with very low to zero Ti content. In the olivine hornblendites, some hornblendes are mantled by acicular cummingtonite. Both actinolite and cummingtonite also occur as individual acicular crystals as well as overgrowths. The presence of these minerals indicates sub-solidus alteration of the primary magmatic assemblage. Cummingtonite may form through alteration of orthopyroxene at temperatures below 800°C (Fonorev & Korolkov, 1980). Hornblende in the gabbros and diorites sometimes hosts small anhedral blebs of quartz. These are commonly surrounded by zones of actinolite or actinolitic hornblende—textures similar to those seen in the granodiorite–tonalite unit. In the diorites, the hornblende is less magnesian than in the mafic and ultramafic rocks. It occurs as euhedra or clusters of anhedral crystals between 20 and 40 mm across with the same compositions. The euhedra are sometimes zoned with cores of actinolitic hornblende mantled by magnesio-hornblende. Some diorite samples contain euhedral magnesio-hornblende crystals devoid of quartz inclusions, suggesting direct amphibole precipitation from $H_2O$-rich melt.

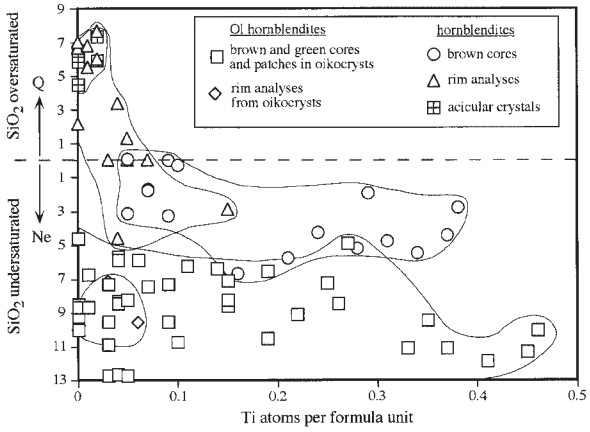


**Fig. 7.** Plot of CIPW normative Ne and Q vs Ti atoms p.f.u. for calcic amphiboles from the olivine hornblendites and hornblendites. Compositions that plot along the dotted line at Ne = Q = zero are hypersthene normative. CIPW norms calculated assuming $Fe^{3+}/Fe_{total} = 0{\cdot}25$.

Biotite compositions are shown graphically in Fig. 5, and representative analyses are given in Table 3. Biotite becomes less magnesian from the olivine hornblendites to the diorites. It occurs interstitially to hornblende crystals in the olivine hornblendites and also poikilitically encloses olivine crystals, indicating late crystallization. In the mafic and intermediate rocks, biotite occurs as individual plates and anhedral patches replacing hornblende. The biotite is less magnesian than the coexisting hornblende. In the olivine hornblendites, there is some sub-solidus alteration of biotite to clinochlore.

Olivine is present only in the olivine hornblendites. Its composition is $Fo_{68–83}$ and the crystals are up to 2 mm across. The olivine crystals are generally close together, sometimes touching, and are distributed fairly evenly throughout the samples and sometimes host small inclusions of spinel. Where biotite is altered to clinochlore, the olivine is pseudomorphed by talc.

## MINERALOGICAL CONSTRAINTS ON EMPLACEMENT DEPTH OF THE QUÉRIGUT MASSIF

Constraints on the emplacement depth of the Massif are obtained from petrographic observations on rocks of the narrow thermal aureole characterized by metapelitic hornfelses and skarns. In the metapelites, the mineral assemblage andalusite and K-feldspar has formed through the reaction

$$Ms + Qtz = Als + Kfs + H_2O.$$

This reaction is plotted in $P$–$T$ space in Fig. 8 using experimental data from Althaus *et al.* (1970), Kerrick (1972) and Chatterjee & Froese (1975). The two curves for the 'muscovite out' reaction are drawn at values of $XH_2O = 1$ and 0·8. The choice of this range for the fluid composition is based on the occurrence of the assemblage Grs + Cc + Qtz in the skarns, which indicates $XH_2O$ of (0·88 (Tracy & Frost, 1991). The observation that abundant muscovite occurs in the metapelites, suggesting the presence of an externally derived aqueous fluid buffering the reaction, also supports this choice of values. Figure 8 shows that the mineral assemblage in the metapelitic hornfelses points to a maximum emplacement pressure for the Quérigut Massif of around 260–270 MPa.

## MAJOR AND TRACE ELEMENT GEOCHEMISTRY

Full major and trace element compositions of the rocks are given in Table 4. Average compositions of the units are given in Table 5.

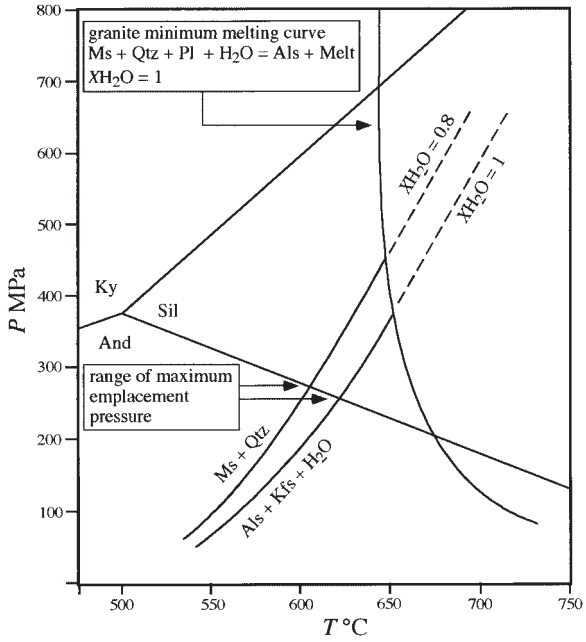


**Fig. 8.** Pressure–temperature plot showing the maximum emplacement pressure of the Quérigut Massif. Stability relations of $Al_2SiO_5$ polymorphs are from Holdaway (1971). Ms + Qtz stability curves taken from Althaus *et al.* (1970), Kerrick (1972) and Chatterjee & Froese (1975). Granite minimum melting curve from Piwinskii (1968).

### Major elements

The calc-alkaline chemistry of the rocks is illustrated in Fig. 9, a plot of wt % $K_2O$ vs wt % $SiO_2$, which includes the field boundaries of Peccerillo & Taylor (1976). Here, the biotite granite and monzogranite units plot in the field that defines high-K calc-alkaline rocks, whereas the granodiorite–tonalite unit plots dominantly in the normal-K calc-alkaline field. The diorites straddle the boundaries between these two fields.

The degree of alumina saturation in the rocks is shown in Fig. 10, a plot of molar A/CNK vs wt % $SiO_2$. Data for the diorites to biotite granite form a roughly linear trend of increasing A/CNK with increasing $SiO_2$. The granitic rocks are mostly metaluminous and fall within the field of I-type granites, with A/CNK <1·1 (Chappell & White, 1974). The shift in the A/CNK ratio of some ultramafic rocks towards more aluminous values is due to varying degrees of sub-solidus alteration.

A range of other major element variation diagrams is shown in Fig. 11. The plots of wt % FeO* and MgO vs wt % $SiO_2$ broadly show decreasing MgO and FeO* with increasing $SiO_2$. In addition, in the plot of MgO vs $SiO_2$ there appear to be two trends: a high-MgO trend that corresponds to the ultramafic rocks, hornblende gabbros and diorites, and a low-MgO trend followed by

*Table 4: Major element and trace element compositions of the samples*

| Rock type: | Bt tonalite | foliated Hbl–Bt granodiorite | Bt tonalite | Hbl–Bt granodiorite | Bt tonalite | Bt tonalite | foliated Bt tonalite | Bt tonalite | Bt tonalite | Or-phyric monzogranite |
|---|---|---|---|---|---|---|---|---|---|---|
| Sample: | QH29 | QH56 | QH70 | QH76 | QH107 | QH146 | QH170 | QH214 | QH217 | QH13 |
| $SiO_2$ | 62·74 | 60·50 | 60·32 | 64·79 | 68·2 | 62·10 | 56·25 | 62·73 | 63·14 | 71·92 |
| $TiO_2$ | 0·75 | 0·75 | 0·66 | 0·64 | 0·45 | 0·73 | 1·30 | 0·69 | 0·78 | 0·36 |
| $Al_2O_3$ | 17·47 | 17·31 | 17·36 | 16·87 | 16·48 | 17·94 | 17·72 | 17·28 | 17·59 | 14·65 |
| FeO* | 4·25 | 6·46 | 5·16 | 4·49 | 2·98 | 4·28 | 7·69 | 5·07 | 4·60 | 2·38 |
| MnO | 0·18 | 0·20 | 0·22 | 0·21 | 0·18 | 0·15 | 0·27 | 0·19 | 0·18 | 0·16 |
| MgO | 1·91 | 3·25 | 2·10 | 1·72 | 1·16 | 2·11 | 4·18 | 1·83 | 2·36 | 0·66 |
| CaO | 6·40 | 5·89 | 7·30 | 4·80 | 3·89 | 6·89 | 7·15 | 5·83 | 6·05 | 2·49 |
| $Na_2O$ | 4·50 | 3·35 | 5·05 | 3·79 | 3·79 | 4·12 | 3·24 | 4·43 | 3·35 | 3·44 |
| $K_2O$ | 1·61 | 2·14 | 1·56 | 2·53 | 2·69 | 1·49 | 1·91 | 1·78 | 1·75 | 3·78 |
| $P_2O_5$ | 0·18 | 0·15 | 0·27 | 0·15 | 0·18 | 0·20 | 0·29 | 0·17 | 0·19 | 0·17 |
| Nb | 12 | 16 | 14 | 13 | 15 | 12 | 22 | 16 | 14 | 18 |
| Zr | 305 | 219 | 318 | 243 | 224 | 333 | 332 | 279 | 276 | 188 |
| Y | 32 | 46 | 40 | 43 | 31 | 27 | 51 | 37 | 33 | 43 |
| Sr | 477 | 281 | 534 | 318 | 216† | 435 | 368† | 299† | 341 | 151† |
| Rb | 76 | 107 | 62 | 100 | 82† | 82 | 78† | 60† | 88 | 167† |
| Zn | 46 | 76 | 57 | 63 | 50 | 64 | 68 | 70 | 52 | 40 |
| Cu | b.d. | 5 | 4 | 2 | 1 | 17 | 7 | 5 | 5 | 6 |
| Ni | 2 | 15 | b.d. | b.d. | b.d. | b.d. | 6 | b.d. | 1 | b.d. |
| Cr | 30 | 88 | 39 | 29 | 23 | 32 | 54 | 29 | 38 | 13 |
| Ce | 94 | 93 | 88 | 97 | 43 | 37 | 91 | 93 | 96 | 66 |
| Nd | 29 | 31 | 31 | 31 | 14† | 11 | 35† | 28† | 26 | 35† |
| V | 64 | 110 | 83 | 79 | 39 | 71 | 152 | 83 | 79 | 40 |
| La | 41 | 38 | 39 | 41 | 36 | 24 | 49 | 48 | 37 | 51 |
| Ba | 534 | 487 | 603 | 848 | 245 | 524 | 679 | 739 | 592 | 499 |
| Sc | 4 | 15 | 25 | 10 | 9 | 9 | 23 | 12 | 10 | 4 |
| A/CNK | 0·88 | 0·97 | 0·79 | 1·00 | 1·07 | 0·90 | 0·90 | 0·92 | 1·00 | 1·09 |
| *mg*-no. | 44·5 | 47·3 | 42·0 | 40·6 | 41·0 | 46·8 | 49·2 | 39·2 | 47·8 | 33·1 |

the felsic rocks. This feature is not apparent in the FeO* vs $SiO_2$ plot, where the data form a gently concave array that might be taken as suggestive of fractional crystallization.

In contrast, on plots of wt % CaO, $Al_2O_3$, $Na_2O$ and $TiO_2$ vs wt % $SiO_2$ the data form bell-shaped arrays. Very broadly, the plots show an increase in these oxides with increasing $SiO_2$ through the ultramafic rocks to the diorites, and a decrease with increasing $SiO_2$ through the felsic series. An important feature is the presence of compositional gaps separating the diorites, hornblende gabbros and ultramafic rocks from the felsic series. This is most apparent on the plot of wt % $Na_2O$ vs wt % $SiO_2$, and is also noticeable on the $TiO_2$ vs $SiO_2$ plot. On the plot of $Al_2O_3$ vs wt % $SiO_2$, the compositional gap separates the hornblende gabbros and ultramafic rocks from the diorites and the felsic series. It should be noted that there are no corresponding gaps in $SiO_2$ content. In terms of major element geochemistry, there appears to be little difference in composition between the monzogranite and the biotite granite units.

## Trace elements

Variation diagrams for selected trace elements are given in Fig. 12. The plots of Ba, Sr and Zr vs wt % $SiO_2$ have bell-shaped data arrays similar to those for some of the major elements. This indicates that these elements behave incompatibly through the ultramafic to intermediate series, and compatibly during crystallization of

*Table 4: continued*

| Rock type: | Mc-phyric monzo-granite | Or-phyric monzo-granite | Mc-phyric monzo-granite | Kfs-phyric monzo-granite | Kfs-phyric monzo-granite | Mc-phyric monzo-granite | Mc-phyric monzo-granite | Or- aphyric monzo-granite | Mc-phyric monzo-granite | Or-bearing Bt granite |
|---|---|---|---|---|---|---|---|---|---|---|
| Sample: | QH34 | QH45 | QH53 | QH126 | QH130 | QH133 | QH148 | QH239 | QH241 | QH89 |
| $SiO_2$ | 72·09 | 67·55 | 72·12 | 75·59 | 73·51 | 72·23 | 70·82 | 69·85 | 69·03 | 73·30 |
| $TiO_2$ | 0·41 | 0·45 | 0·18 | 0·37 | 0·15 | 0·32 | 0·35 | 0·40 | 0·40 | 0·18 |
| $Al_2O_3$ | 14·44 | 16·55 | 15·27 | 11·93 | 13·50 | 13·75 | 15·20 | 15·56 | 15·78 | 14·73 |
| FeO* | 2·63 | 3·19 | 1·70 | 2·97 | 1·73 | 2·34 | 2·20 | 2·77 | 2·54 | 1·89 |
| MnO | 0·10 | 0·10 | 0·10 | 0·14 | 0·12 | 0·13 | 0·16 | 0·19 | 0·19 | 0·11 |
| MgO | 0·80 | 1·10 | 0·37 | 1·07 | 0·37 | 0·83 | 0·80 | 1·20 | 0·99 | 0·41 |
| CaO | 2·87 | 3·64 | 1·83 | 1·74 | 1·43 | 2·05 | 2·51 | 3·17 | 2·54 | 1·51 |
| $Na_2O$ | 3·86 | 3·85 | 3·86 | 2·85 | 4·28 | 3·55 | 3·99 | 3·11 | 3·60 | 3·59 |
| $K_2O$ | 2·62 | 3·43 | 4·48 | 3·23 | 4·83 | 4·68 | 3·86 | 3·65 | 4·81 | 4·22 |
| $P_2O_5$ | 0·17 | 0·13 | 0·08 | 0·12 | 0·07 | 0·10 | 0·12 | 0·09 | 0·13 | 0·07 |
| Nb | 22 | 14 | 18 | 21 | 19 | 21 | 20 | 14 | 16 | 24 |
| Zr | 193 | 207 | 138 | 180 | 120 | 150 | 164 | 185 | 181 | 127 |
| Y | 43 | 48 | 47 | 57 | 57 | 43 | 41 | 41 | 43 | 56 |
| Sr | 210 | 252 | 134 | 124 | 95 | 183 | 210 | 142† | 141† | 80† |
| Rb | 155 | 148 | 181 | 153 | 252 | 189 | 167 | 134† | 159† | 235† |
| Zn | 47 | 54 | 32 | 49 | 38 | 28 | 28 | 40 | 42 | 36 |
| Cu | b.d. | 5 | b.d. | 26 | 22 | 19 | 15 | b.d. | 7 | 4 |
| Ni | 2 | b.d. | b.d. | 2 | b.d. | b.d. | b.d. | b.d. | b.d. | 1 |
| Cr | 16 | 23 | 9 | 31 | 2 | 10 | 12 | 12 | 14 | 9 |
| Ce | 81 | 118 | 78 | 185 | 102 | 74 | 63 | 117 | 145 | 55 |
| Nd | 25 | 34 | 29 | 33 | 22 | 26 | 19 | 29† | 46† | 22† |
| V | 39 | 52 | 18 | 33 | 12 | 35 | 32 | 36 | 38 | 15 |
| La | 32 | 62 | 39 | 38 | 41 | 37 | 43 | 44 | 66 | 27 |
| Ba | 359 | 791 | 434 | 213 | 310 | 681 | 683 | 632 | 719 | 325 |
| Sc | 4 | 12 | 2 | 3 | 9 | b.d. | b.d. | 10 | 3 | 9 |
| A/CNK | 1·07 | 1·05 | 1·12 | 1·12 | 0·97 | 0·99 | 1·06 | 1·10 | 1·06 | 1·19 |
| *mg*-no. | 35·2 | 38·1 | 28·0 | 39·1 | 27·6 | 38·7 | 39·3 | 43·6 | 41·0 | 27·9 |

the felsic series. In contrast, Rb increases with increasing $SiO_2$ throughout the suite, and marked gaps separate the granodiorite–tonalites from the monzogranites, and the monzogranites from the biotite granites. The Rb contents of biotite granites are much higher at comparable $SiO_2$ contents than those of the monzogranites. The trace element variation among the units of the Massif shows marked compositional discontinuities similar to those among the major elements. What is noticeable in all the trace element variation diagrams is that each unit appears to plot more or less in its own compositional space. This is unlikely to be an artefact of sampling, as every effort was made to collect representative samples covering the range of rock types observed in the field.

The hornblende gabbros and ultramafic rocks have very high Cr and Ni contents (Fig. 12). These plots have logarithmic scales on their vertical axes to facilitate better data dispersion. Comparison of the compositions of the hornblende gabbros with basalts of similar $SiO_2$ and MgO contents shows that the concentrations of these trace elements are much higher than in normal basaltic magmas. The Cr and Ni contents of the olivine hornblendites and hornblendites fall within the range of similar ultramafic rocks commonly interpreted as having been formed as mafic mineral cumulates. By similar reasoning, it appears probable that a cumulate component is present in the hornblende gabbros. This is probably in the form of spinel, as only a slight variation in the modal content

| Rock type: | Or-bearing Bt granite | Pl-phyric Hbl–Bt diorite | Hbl-phyric diorite | Pl-phyric diorite | Bt-phyric diorite | Pl-phyric Hbl–Bt diorite | Pl-phyric diorite | Pl-phyric diorite | Hbl gabbro | Hbl gabbro |
|---|---|---|---|---|---|---|---|---|---|---|
| Sample: | QH127 | QM50 | QM109 | QM138 | QM197 | QM213 | QM228 | QM236 | QM77 | QM119 |
| $SiO_2$ | 73·83 | 55·61 | 53·93 | 55·27 | 53·06 | 52·07 | 56·78 | 55·44 | 51·58 | 49·69 |
| $TiO_2$ | 0·16 | 0·79 | 1·31 | 0·74 | 1·01 | 0·99 | 1·25 | 0·83 | 0·50 | 0·63 |
| $Al_2O_3$ | 14·04 | 16·59 | 17·07 | 15·62 | 17·25 | 17·08 | 17·44 | 16·88 | 10·31 | 8·84 |
| FeO* | 1·83 | 7·13 | 7·63 | 6·86 | 8·73 | 8·45 | 7·34 | 7·10 | 9·73 | 11·86 |
| MnO | 0·10 | 0·23 | 0·21 | 0·22 | 0·24 | 0·21 | 0·21 | 0·26 | 0·20 | 0·20 |
| MgO | 0·37 | 6·12 | 6·85 | 8·22 | 6·63 | 7·65 | 4·27 | 6·31 | 15·98 | 20·2 |
| CaO | 1·42 | 8·65 | 8·67 | 8·39 | 9·87 | 10·49 | 7·15 | 9·01 | 8·96 | 6·87 |
| $Na_2O$ | 3·76 | 2·61 | 2·62 | 2·76 | 1·44 | 1·55 | 3·35 | 1·96 | 1·36 | 0·82 |
| $K_2O$ | 4·43 | 2·12 | 1·57 | 1·75 | 1·59 | 1·34 | 1·87 | 2·07 | 1·28 | 0·74 |
| $P_2O_5$ | 0·06 | 0·15 | 0·14 | 0·16 | 0·17 | 0·17 | 0·34 | 0·15 | 0·10 | 0·14 |
| Nb | 19 | 15 | 17 | 13 | 14 | 16 | 25 | 13 | 9 | 10 |
| Zr | 118 | 142 | 168 | 148 | 129 | 265 | 240 | 169 | 93 | 98 |
| Y | 63 | 47 | 49 | 63 | 55 | 53 | 54 | 49 | 42 | 41 |
| Sr | 70† | 241 | 550 | 300† | 237† | 375 | 418 | 192† | 141 | 136† |
| Rb | 247† | 103 | 71 | 71† | 65† | 67 | 90 | 93† | 68 | 31† |
| Zn | 42 | 71 | 70 | 63 | 76 | 89 | 69 | 72 | 77 | 66 |
| Cu | b.d. | 3 | 32 | 33 | 20 | 28 | 23 | 16 | 21 | 59 |
| Ni | 2 | 13 | 10 | 89 | 13 | 14 | b.d. | 18 | 182 | 343 |
| Cr | 6 | 131 | 132 | 251 | 102 | 167 | 47 | 128 | 1249 | 2022 |
| Ce | 54 | 52 | 60 | 46 | 73 | 67 | 103 | 63 | 47 | 20 |
| Nd | 20† | 25 | 20 | 28† | 25† | 23 | 44 | 18† | 9 | 12† |
| V | 10 | 164 | 246 | 145 | 215 | 211 | 154 | 166 | 168 | 146 |
| La | 47 | 20 | 18 | 22 | 30 | 28 | 33 | 29 | 21 | 24 |
| Ba | 309 | 391 | 355 | 256 | 347 | 357 | 479 | 336 | 219 | 93 |
| Sc | 4 | 24 | 31 | 29 | 34 | 37 | 21 | 32 | 37 | 25 |
| A/CNK | 1·11 | 0·76 | 0·81 | 0·74 | 0·79 | 0·75 | 0·88 | 0·79 | 0·53 | 0·61 |
| *mg*-no. | 26·5 | 60·5 | 61·5 | 68·1 | 57·5 | 61·7 | 50·9 | 61·3 | 74·5 | 75·2 |

of this mineral would produce a pronounced effect on the Cr and Ni contents of the rocks.

A cumulate origin for the ultramafic rocks is also suggested in Fig. 13a and b, which present the results of Rayleigh fractionation modelling of Sr, Rb and Ba. In these diagrams, the Sr, Rb and Ba contents of these rocks could be explained by the accumulation of hornblende and olivine from a mafic magma corresponding broadly to the hornblende gabbro. The marked effect that the presence of minor amounts of olivine can have on the compositions of these rocks should be noted. The two olivine hornblendite samples with low Sr contents are altered, whereas the sample with high Sr is due to the presence of plagioclase. Evolved liquids from fractional crystallization of the mafic magma could be represented by the diorites. Alternatively, the variation in Fig. 13a and b suggests that some of the diorites may represent cumulates of plagioclase and hornblende (or clinopyroxene) from granodioritic–tonalitic magma, particularly the sample with the highest Sr content (QM109).

Similarly, the data dispersion suggests that the granodiorite–tonalite unit could have formed through mineral accumulation from the crystallizing monzogranite magma. The negative slope of the data through the granodiorite–tonalites and monzogranite in Fig. 13a seems to point to the role played by feldspar fractionation in the formation of these rocks. In Fig. 13b, the plagioclase and K-feldspar vectors are resolved, and the comagmatic relationship between the granodiorite–tonalites and monzogranites can be modelled by plagioclase accumulation

*Table 4: continued*

| Rock type: | Hbl gabbro | hornblendite | Ol–Phl hornblendite | Ol–Phl hornblendite | Ol–Phl hornblendite | Ol–Phl hornblendite | hornblendite | Ol–Phl hornblendite | Ol–Phl hornblendite |
|---|---|---|---|---|---|---|---|---|---|
| Sample: | QM144 | QUM5 | QUM6 | QUM7(1) | QUM8 | QUM64 | QUM68 | QUM71 | QUM226 |
| $SiO_2$ | 51·18 | 47·75 | 45·74 | 45·34 | 44·50 | 46·18 | 46·72 | 46·86 | 36·36 |
| $TiO_2$ | 0·49 | 0·65 | 0·33 | 0·32 | 0·33 | 0·47 | 0·64 | 0·44 | 0·29 |
| $Al_2O_3$ | 11·53 | 9·26 | 7·11 | 7·10 | 7·01 | 7·69 | 9·78 | 7·48 | 6·58 |
| FeO* | 8·28 | 12·21 | 12·30 | 12·72 | 12·11 | 12·07 | 11·67 | 11·80 | 27·22 |
| MnO | 0·19 | 0·20 | 0·19 | 0·18 | 0·23 | 0·18 | 0·20 | 0·19 | 0·11 |
| MgO | 14·31 | 21·97 | 28·70 | 28·90 | 30·49 | 28·97 | 22·08 | 28·30 | 25·18 |
| CaO | 12·4 | 7·19 | 4·13 | 4·03 | 4·92 | 3·61 | 8·27 | 3·65 | 3·44 |
| $Na_2O$ | 1·21 | 0·54 | 0·67 | 0·84 | 0·27 | 0·22 | 0·35 | 0·63 | 0·35 |
| $K_2O$ | 0·33 | 0·09 | 0·76 | 0·51 | 0·08 | 0·52 | 0·13 | 0·53 | 0·43 |
| $P_2O_5$ | 0·07 | 0·13 | 0·06 | 0·07 | 0·06 | 0·09 | 0·15 | 0·12 | 0·03 |
| Nb | 9 | 8 | 11 | 6 | 10 | 10 | 13 | 11 | 6 |
| Zr | 80 | 89 | 56 | 53 | 46 | 79 | 122 | 103 | 94 |
| Y | 41 | 41 | 34 | 32 | 31 | 35 | 40 | 34 | 44 |
| Sr | 117† | 64 | 77 | 67† | 43 | 48 | 50 | 101† | 210 |
| Rb | 13† | b.d. | 43 | 22† | 4 | 21 | 1 | 19† | 43 |
| Zn | 67 | 73 | 75 | 86 | 54 | 76 | 80 | 83 | 127 |
| Cu | 46 | 10 | 58 | 42 | 39 | 40 | b.d. | 54 | 78 |
| Ni | 90 | 348 | 988 | 985 | 300 | 596 | 879 | 1272 | 546 |
| Cr | 1399 | 2330 | 3554 | 3835 | 2686 | 2067 | 2060 | 4017 | 2463 |
| Ce | 33 | 26 | 5 | 6 | 9 | 9 | 4 | 19 | 7 |
| Nd | 6† | 5 | b.d. | 6† | 1 | b.d. | 6 | 12† | b.d. |
| V | 216 | 148 | 103 | 105 | 81 | 100 | 112 | 101 | 102 |
| La | 21 | 20 | 30 | 32 | 7 | 23 | 27 | 24 | 14 |
| Ba | 42 | b.d. | 103 | 50 | b.d. | 30 | b.d. | 84 | 38 |
| Sc | 58 | 23 | 20 | 14 | 22 | 19 | 16 | 9 | 23 |
| A/CNK | 0·47 | 0·66 | 0·77 | 0·78 | 0·74 | 1·03 | 0·62 | 0·92 | 0·91 |
| *mg*-no. | 75·5 | 76·2 | 80·6 | 80·2 | 81·8 | 81·1 | 77·1 | 81·0 | 62·3 |

All analyses were obtained by XRF spectroscopy unless otherwise specified. Major element oxides are reported as 100 wt % anhydrous, and trace elements in ppm by wt. FeO*, total Fe as FeO; *mg*-number = 100[molar Mg/(Mg + Fe)]; A/CNK = molar $Al_2O_3/(CaO + Na_2O + K_2O)$; b.d., below detection limit.
†Concentrations obtained from isotope dilution and mass spectrometry.

in the former. In addition, the variation of the monzogranite seems best explained by K-feldspar fractionation. However, this is unlikely, as the rock textures indicate that K-feldspar is late crystallizing, and thus would not be expected to exert any major control on the Ba contents until a late stage in crystallization.

Apparent linear trends within the data dispersion of each unit could well be evidence that the various magma parcels underwent closed-system fractional crystallization dominated by plagioclase and alkali feldspar. The dispersion of the diorite data appears to have been caused by hornblende and/or clinopyroxene as well as plagioclase. In contrast to the wide spread of the compositions of the other rocks, the biotite granite plots in a very restricted compositional space and appears to be a homogeneous magma batch.

Overall, the features shown by the trace element chemistry appear to favour the existence of up to four independent magma batches. However, data dispersions also support other processes such as fractional crystallization, mixing, unmixing, or combined assimilation and fractional crystallization. Any comagmatic re-

*Table 5: Average major element and trace element compositions of the Quérigut rocks*

| | Average gd–ton | Average monz | Average biotite granite | Average diorite | Average hornblende gabbro | Average Ol hbl | Average hbl |
|---|---|---|---|---|---|---|---|
| $SiO_2$ | 62·31 | 71·47 | 73·57 | 54·59 | 50·82 | 44·93 | 47·24 |
| $TiO_2$ | 0·75 | 0·34 | 0·17 | 0·99 | 0·54 | 0·43 | 0·65 |
| $Al_2O_3$ | 17·34 | 14·66 | 14·39 | 16·85 | 10·23 | 7·75 | 9·52 |
| FeO* | 5·00 | 2·45 | 1·86 | 7·61 | 9·96 | 14·01 | 11·94 |
| MnO | 0·20 | 0·14 | 0·11 | 0·23 | 0·20 | 0·19 | 0·20 |
| MgO | 2·29 | 0·82 | 0·39 | 6·58 | 16·83 | 26·82 | 22·03 |
| CaO | 6·02 | 2·43 | 1·47 | 8·89 | 9·41 | 4·91 | 7·73 |
| $Na_2O$ | 3·96 | 3·64 | 3·68 | 2·33 | 1·13 | 0·48 | 0·45 |
| $K_2O$ | 1·94 | 3·94 | 4·33 | 1·76 | 0·78 | 0·38 | 0·11 |
| $P_2O_5$ | 0·20 | 0·12 | 0·07 | 0·18 | 0·10 | 0·09 | 0·14 |
| Nb | 15 | 18 | 22 | 16 | 9 | 9 | 11 |
| Zr | 281 | 171 | 123 | 180 | 90 | 80 | 106 |
| Y | 38 | 46 | 60 | 53 | 41 | 36 | 41 |
| Sr | 363 | 164 | 75 | 330 | 131 | 90 | 57 |
| Rb | 82 | 171 | 241 | 80 | 37 | 19 | 1 |
| Zn | 61 | 40 | 39 | 73 | 70 | 82 | 77 |
| Cu | 6 | 14 | 4 | 22 | 42 | 40 | 5 |
| Ni | 6 | 2 | 2 | 26 | 205 | 739 | 614 |
| Cr | 40 | 14 | 8 | 137 | 1557 | 2877 | 2195 |
| Ce | 81 | 103 | 55 | 66 | 33 | 11 | 15 |
| Nd | 26 | 30 | 21 | 26 | 9 | 3 | 6 |
| V | 84 | 34 | 13 | 186 | 177 | 107 | 130 |
| La | 39 | 45 | 37 | 26 | 22 | 22 | 24 |
| Ba | 583 | 532 | 317 | 360 | 118 | 38 | b.d. |
| Sc | 13 | 6 | 7 | 30 | 40 | 18 | 20 |
| A/CNK | 0·94 | 1·06 | 1·15 | 0·79 | 0·54 | 0·86 | 0·64 |
| *mg*-no. | 44·3 | 36·4 | 27·2 | 60·2 | 75·1 | 77·5 | 76·68 |
| *n* | 9 | 10 | 3 | 7 | 3 | 6 | 2 |

Major element oxides are reported as 100 wt % anhydrous, and trace elements in ppm by wt. (For further details, see Table 4 caption.) gd–ton, granodiorite–tonalite; monz, monzonite; hbl, hornblendite; *n*, number of analyses.

lationships between the units should be apparent from their isotope systematics. These are examined below.

## ISOTOPE GEOCHEMISTRY

### U–Pb zircon geochronology

A tonalite sample, QZ233, from the granodiorite–tonalite unit was chosen for this part of the study, because the most mafic granitic rocks are least likely to contain inherited components in their zircons, and hence are best suited for obtaining a concordant age. In the QZ233 tonalite sample, the zircon crystals are light yellow, euhedral, short and prismatic (length-to-width ratio 3–4). No clear magmatic zoning is visible under binocular microscope. Using the classification scheme of Pupin (1980), the morphology of the zircons is typical for those from granodioritic and monzogranitic magmas. Four abraded zircon fractions were analysed and these define a linear array [mean square weighted deviation (MSWD) = 0·1] intersecting the concordia at 307 ± 2 Ma (Table 6 and Fig. 14), the lower intercept being at the origin of the diagram. Fraction 1 is concordant and fractions 2, 3 and 4 are slightly discordant, with no evidence within error of an inherited component. Consequently, the upper intercept at 307 ± 2 Ma is

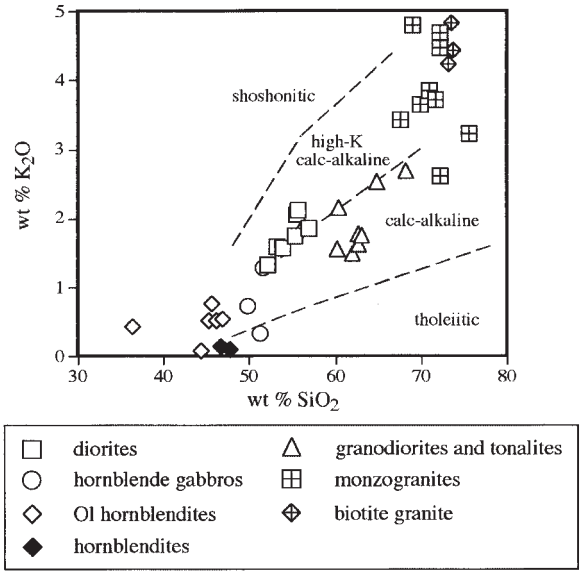


**Fig. 9.** Major element Harker diagram of wt % $K_2O$ vs wt % $SiO_2$. Field boundaries after Peccerillo & Taylor (1976).

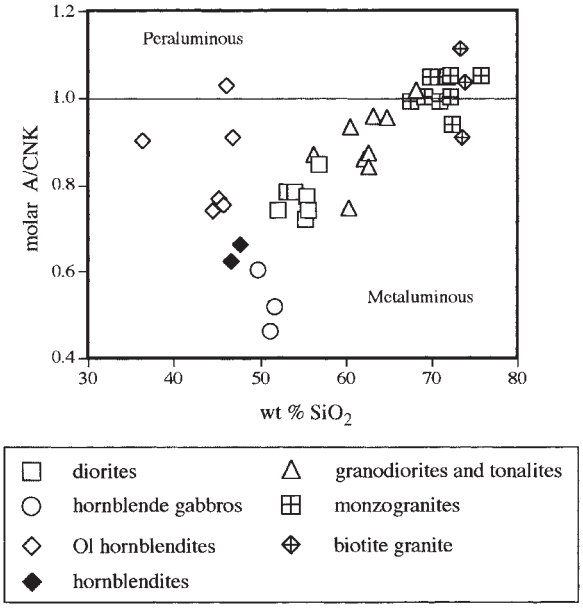


**Fig. 10.** Plot of molar A/CNK vs wt % $SiO_2$. Boundary for metaluminous and peraluminous compositions after Shand (1947). A/CNK is defined as mol $Al_2O_3$/(mol CaO + mol $Na_2O$ + mol $K_2O$).

interpreted as the crystallization age of the QZ233 tonalite magma.

## Rb–Sr isotopes

Rb–Sr analyses of carefully selected, representative samples of the Quérigut rocks are listed in Table 7. The range of initial $^{87}Sr/^{86}Sr$ values suggests that the Massif represents either a comagmatic suite related through AFC (or other mixing processes) or a series of separate magma batches from different sources. None of the rocks have initial Sr isotope ratios typical of the depleted mantle. Figure 15 is a $^{87}Sr/^{86}Sr$ vs $^{87}Rb/^{86}Sr$ isochron plot for the Quérigut rocks. The analyses are bracketed by two reference isochrons calculated at 307 Ma, and the diagram includes a number of isochrons calculated from the data. Isochrons calculated for the mafic to intermediate rocks and combinations thereof have been excluded from the diagram, because of unfeasibly low initial $^{87}Sr/^{86}Sr$ ratios, ages that fall outside of the range realistically expected from the local geology, or very high MSWD values.

The wide spread of apparent ages and initial ratios obtained for the entire dataset or subsets highlights the polygenetic nature of the Massif. The only age similar to the U–Pb zircon age is provided by the combination of data from the felsic series. However, the MSWD value of 41 obtained for this isochron, as well as the others drawn in Fig. 15, provides no statistical validity whatsoever for any of the ages.

Figure 16 is a plot of initial $^{87}Sr/^{86}Sr$ (at 307 Ma) vs 1/Sr, which can be helpful in identifying two-component mixing and AFC-type processes between different magmas, which may result in linear data arrays. The data array on this plot suggests that an origin for the monzogranite by mixing of the diorite and biotite granite magmas is feasible in terms of Sr content and Sr isotopes. The granodiorite–tonalite magma has initial $^{87}Sr/^{86}Sr$ covering the same range as the monzogranite, but with higher Sr contents. This indicates that the granodiorite–tonalite could be either the result of a separate magma batch that produced the monzogranite through fractionation or alternatively a cumulate from a crystallizing monzogranite magma.

Two diorite samples have initial $^{87}Sr/^{86}Sr$ ratios identical to those of the granodiorite–tonalite rocks. This suggests (1) complete Rb–Sr isotope equilibration between the diorites, with initially different $^{87}Sr/^{86}Sr$ signatures, and the granodiorite–tonalite magma, (2) the presence of diorite magmas with the same Rb–Sr isotope signatures as the granodiorites and tonalites, or (3) that the diorites are cumulates from the granodiorite–tonalite magma. Initial $^{87}Sr/^{86}Sr$ ratios of the ultramafic rocks and the hornblende gabbros are broadly similar to that of the least evolved diorites, indicating that these rocks may be linked through fractional crystallization from mafic magmas. Displacement of the Rb/Sr isotopes of these mafic to intermediate rocks away from typical mantle values towards more crustal values may reflect partial Sr isotope equilibration with the surrounding granitoid magmas. However, what is apparent is that the

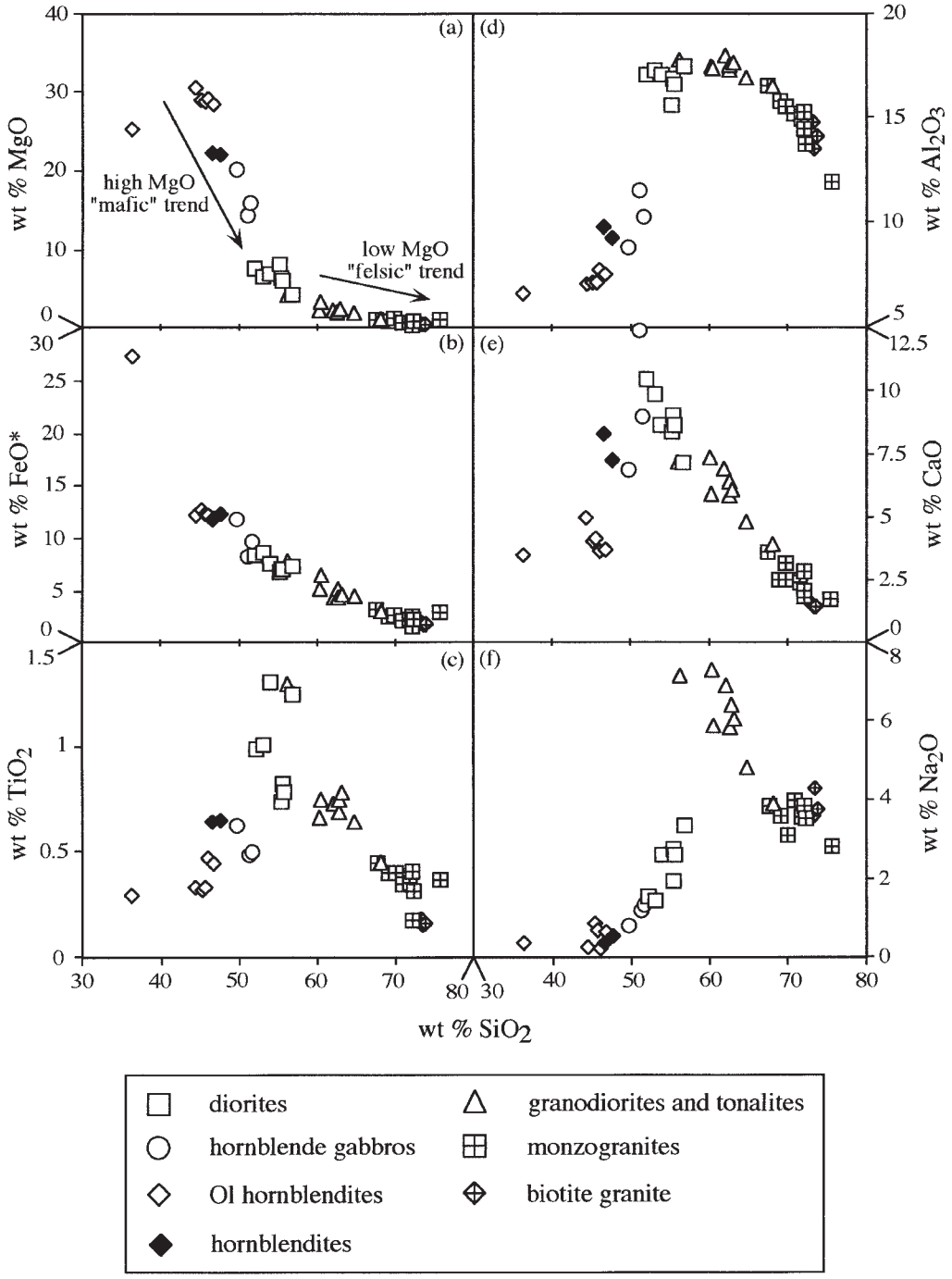


**Fig. 11.** Major element Harker plots of wt % MgO, FeO*, $TiO_2$, $Al_2O_3$, CaO and $Na_2O$ vs wt % $SiO_2$.

wide spread of initial $^{87}Sr/^{86}Sr$ values for the diorites demonstrates that these rocks are polygenetic in origin.

## Sm–Nd isotopes

The results of Sm–Nd isotope analysis on carefully selected, representative samples of the Quérigut rocks are given in Table 8. The wide range of values highlights the general lack of any obvious close genetic relationships between the felsic and mafic rocks. As with the Rb–Sr isotope data, the Sm–Nd data do not show any similarity with depleted mantle values. For the granitic rocks, the data show the dominant role played by crustal material

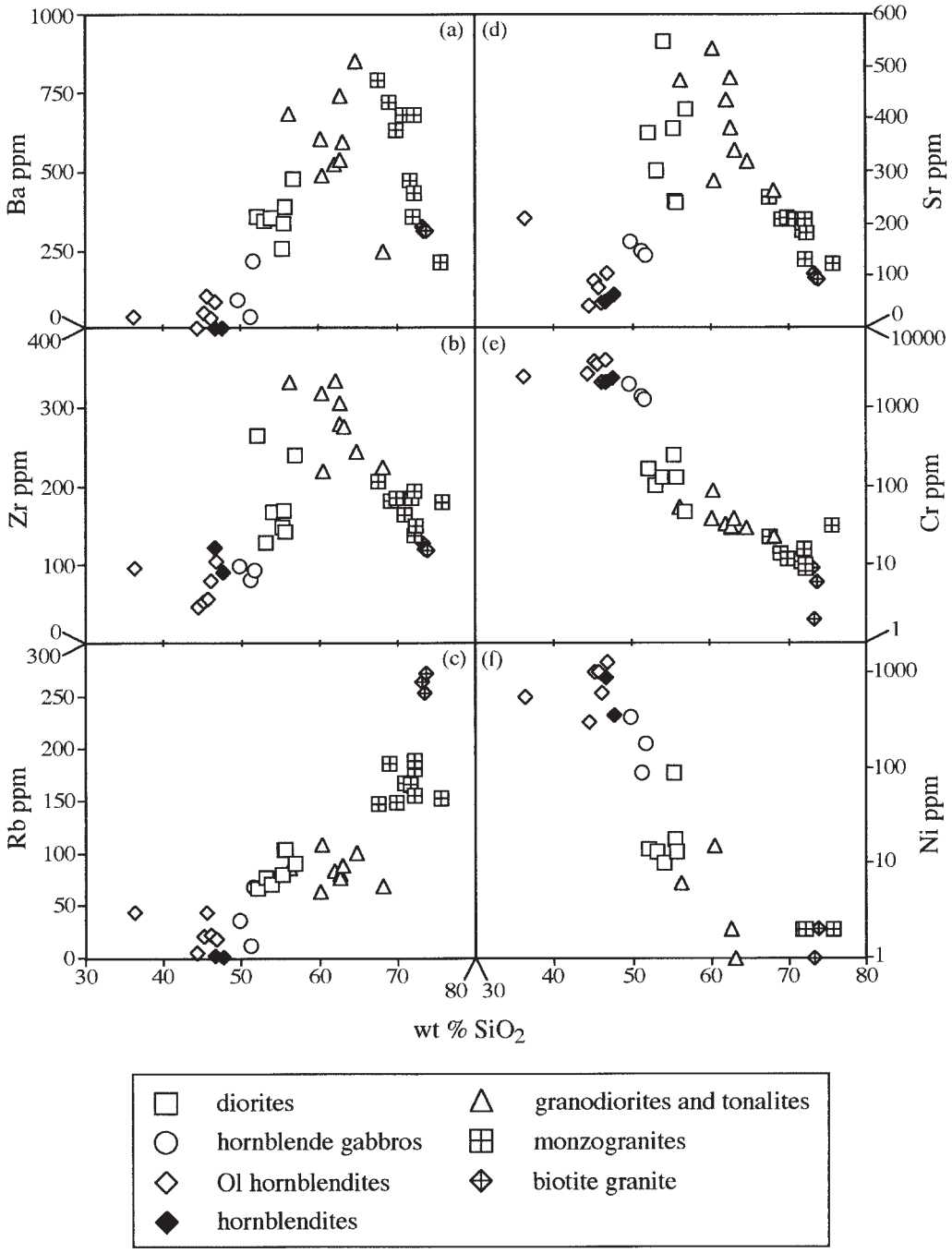


**Fig. 12.** Trace element Harker plots for ppm Ba, Zr, Rb, Sr, Cr and Ni vs wt % $SiO_2$. [Note logarithmic scales in (e) and (f).]

in magma genesis.

Figure 17 is a plot of initial $\varepsilon_{Nd}$ (at 307 Ma) vs initial $^{87}Sr/^{86}Sr$. Also included on the plot for discussion in a later section are fields for published Nd and Sr isotopic values calculated at 307 Ma of other occurrences of magmatic and high-grade metamorphic rocks in the Pyrenees. The biotite granite plots in the extreme lower right corner of the diagram, indicating a source with high time-integrated Rb/Sr and Sm/Nd ratios, typical for crustal rocks. The fields for the granodiorite–tonalite and monzogranite overlap, which indicates either that the two groups are related by closed-system fractionation, or possibly that they were derived from different protoliths with similar time-integrated Rb/Sr and Sm/Nd ratios.

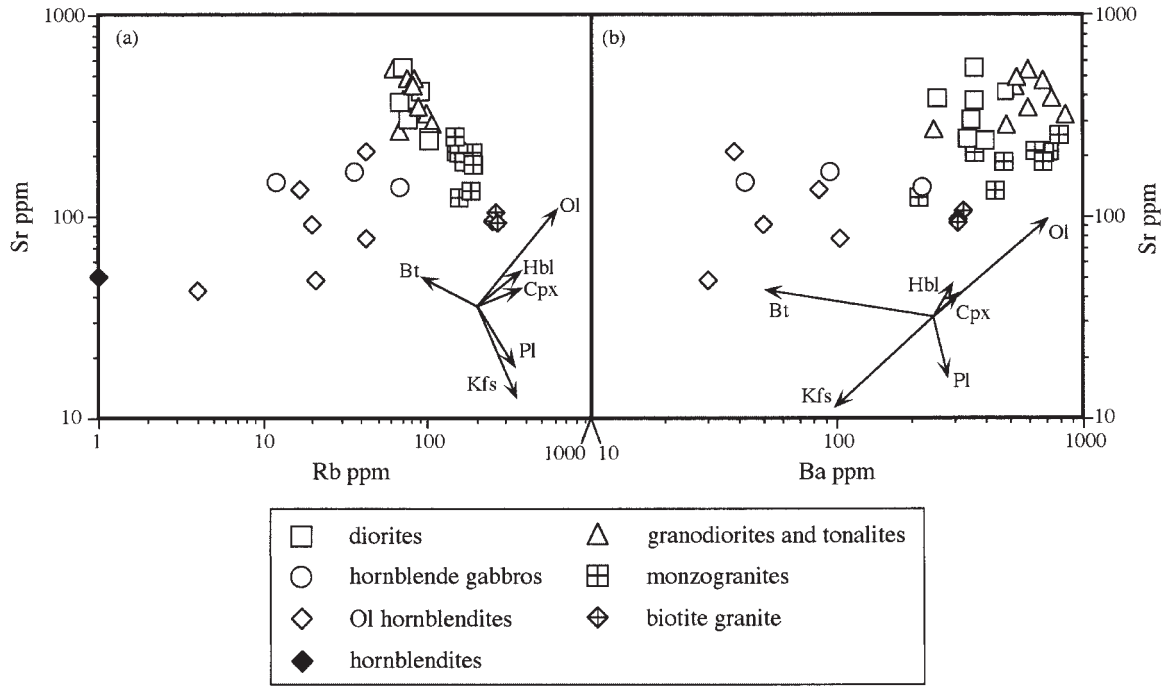


**Fig. 13.** Plots of ppm Sr vs ppm Rb, and ppm Sr vs ppm Ba. Fractional crystallization vectors correspond to 30% Rayleigh fractionation calculated using the $K_d$ values from Rollinson (1993) for basalts (Ol), dacites and rhyolites (other minerals).

*Table 6: U–Pb zircon analysis data for zircons from the granodiorite–tonalite unit*

| Sample | Weight (μg) | Concentration (ppm) | | Atomic ratios | | | | | Apparent ages (Ma) | | |
|---|---|---|---|---|---|---|---|---|---|---|---|
| | | U | Pb* | $^{206}Pb/^{204}Pb$ | $^{208}Pb/^{206}Pb$ | $^{206}Pb/^{238}U$ | $^{207}Pb/^{235}U$ | $^{207}Pb/^{206}Pb$ | $^{206}Pb/^{238}U$ | $^{207}Pb/^{235}U$ | $^{207}Pb/^{206}Pb$ |
| 1: 8 grains | 59 | 584 | 28·2 | 8890 | 0·0997 | 0·04858 ± 13 | 0·3516 ± 8 | 0·05249 ± 2 | 306 | 306 | 307 |
| 2: 7 grains | 55 | 498 | 24·3 | 5886 | 0·1174 | 0·04818 ± 11 | 0·3487 ± 9 | 0·05249 ± 5 | 303 | 304 | 307 |
| 3: 9 grains | 69 | 455 | 22·5 | 2291 | 0·1287 | 0·04797 ± 24 | 0·3470 ± 19 | 0·05246 ± 13 | 302 | 302 | 306 |
| 4: 11 grains | 92 | 623 | 30·7 | 2221 | 0·1291 | 0·04775 ± 36 | 0·3455 ± 27 | 0·05248 ± 9 | 301 | 301 | 307 |

Individual analyses were performed on the least magnetic (3° forward and side tilt at 2·2 A using a Frantz magnetic barrier separator), air-abraded, euhedral, crack-free and initially >75 μm zircon grains. The isotopic ratios are corrected for mass discrimination (0·1% per a.m.u. for Pb and U), isotopic tracer contribution, 5 pg of Pb blank and 0·5 pg of U blank. Initial common Pb is determined using the two-step model of Stacey & Kramers (1975) and uncertainties recommended by Mattinson (1987). The errors on the isotopic ratios are given at the 2σ level. Pb*, radiogenic Pb.

As with the Sr isotopes, the wide range of diorite Nd isotope compositions highlights their polygenetic nature. Two diorite samples have Nd isotope ratios similar to those of the granodiorite–tonalite, indicating either a comagmatic origin or isotopic equilibration of diorite magma with the surrounding granodiorite–tonalite magma. The wide dispersion of the $\varepsilon_{Nd}$ values at 307 Ma for the ultramafic rocks and the hornblende gabbros could reflect heterogeneous mantle source regions beneath the Pyrenees as suggested from gabbros emplaced in the lower crust (Pin, 1989), or varying degrees of isotopic equilibration with the crustal magmas.

## DISCUSSION

The U–Pb zircon age of 307 ± 2 Ma is the first precise constraint for the age of crystallization of the Quérigut Massif. This age is similar to the 303 ± 9 Ma Rb–Sr

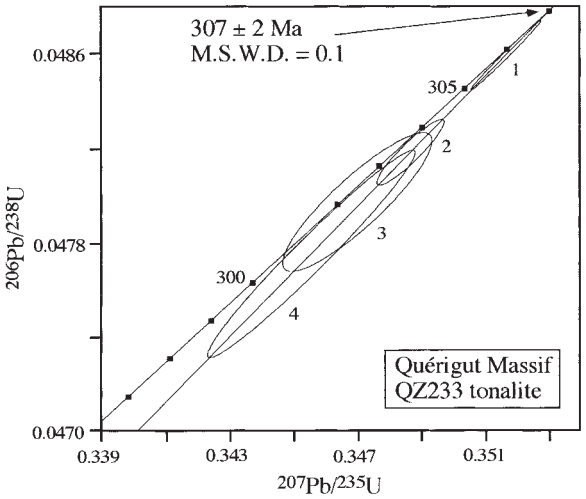


**Fig. 14.** U–Pb concordia diagram for zircons from the granodiorite–tonalite unit. The filled circles along the concordia curve represent intervals of 1 Ma. (See Table 6 for details of the fractions plotted.)

whole-rock isochron obtained on selected samples by Fourcade & Javoy (1991), although it has not been possible to calculate a statistically valid isochron from our own Rb–Sr data, the best fit being 306 ± 10 Ma, MSWD = 41, for the felsic rocks.

The Rb–Sr and Sm–Nd isotope data suggest that the Quérigut rocks cannot represent a single comagmatic sequence as suggested previously (Leterrier, 1972; Marre, 1973), and as might be concluded from some aspects of their major and trace element chemistry. As pointed out by Ben Othman *et al.* (1984), and reinforced by our new data, the Rb–Sr and Sm–Nd isotope data, including model ages, indicate that the granitic rocks were derived essentially through the 'reworking' of older crustal materials.

Major element and trace element geochemistry indicate that the rocks define two main petrogenetic trends: a mafic trend of rapidly decreasing MgO and increasing $Na_2O$, $TiO_2$, Sr, Zr and Ba with increasing $SiO_2$, and a felsic trend of decreasing $Al_2O_3$, $Na_2O$, $TiO_2$, Zr and Sr with increasing $SiO_2$. Definition of the two trends is further supported by the presence of a number of distinct compositional gaps between the mafic and felsic series. Also, there is an overlap in $SiO_2$ contents between some samples of diorite and the granodiorite–tonalite unit. This could result from either crystal segregation in the granodiorite–tonalite magma, forming broadly dioritic cumulates, or formation of slightly more felsic variants of the diorites through fractional crystallization. Other compositional gaps occur in the contents of MgO and Cr between the diorites and the more mafic gabbros and ultramafic rocks (see below).

*Table 7: Rb–Sr isotope composition data of the Quérigut Massif rocks*

| | Rb (ppm) | Sr (ppm) | $^{87}Rb/^{86}Sr$ | $^{87}Sr/^{86}Sr$ | $(^{87}Sr/^{86}Sr)_i$* |
|---|---|---|---|---|---|
| *Diorites* | | | | | |
| QM138 | 71 | 300 | 0·628 | 0·70850 ± 18 | 0·7058 |
| QM197 | 65 | 237 | 0·795 | 0·71296 ± 9 | 0·7095 |
| QM236 | 93 | 192 | 1·401 | 0·71436 ± 11 | 0·7083 |
| *Ol hornblendites* | | | | | |
| QUM7(1) | 22 | 67 | 0·937 | 0·71189 ± 9 | 0·7078 |
| QUM71 | 19 | 101 | 0·531 | 0·70782 ± 8 | 0·7055 |
| *Hornblende gabbros* | | | | | |
| QM119 | 31 | 136 | 0·651 | 0·70869 ± 16 | 0·7059 |
| QM144 | 13 | 117 | 0·329 | 0·70962 ± 27 | 0·7082 |
| *Granodiorite–tonalites* | | | | | |
| QH107 | 82 | 216 | 1·102 | 0·71372 ± 9 | 0·7089 |
| QH214 | 60 | 299 | 0·584 | 0·71209 ± 10 | 0·7096 |
| QH170 | 78 | 368 | 0·611 | 0·71183 ± 10 | 0·7092 |
| *Monzogranites* | | | | | |
| QH239 | 134 | 142 | 2·477 | 0·71925 ± 20 | 0·7085 |
| QH241 | 159 | 141 | 2·953 | 0·72191 ± 27 | 0·7091 |
| QH35 | 124 | 108 | 3·353 | 0·72366 ± 64 | 0·7091 |
| QH13 | 167 | 151 | 3·212 | 0·72253 ± 20 | 0·7086 |
| *Biotite granites* | | | | | |
| QH127 | 247 | 70 | 10·25 | 0·75463 ± 18 | 0·7101 |
| QH89 | 235 | 80 | 8·55 | 0·74839 ± 57 | 0·7113 |

During the course of the analyses international standard NBS 987 gave $^{87}Sr/^{86}Sr$ = 0·710205 ± 0·000015 (2σ) on 19 measurements. The raw data were treated using the normalization values and decay constants recommended by Steiger & Jäger (1977). Errors are quoted at 2σ level.
*$(^{87}Sr/^{86}Sr)_i$ is initial $^{87}Sr/^{86}Sr$ calculated at 307 Ma.

## Mafic series

Compared with the granitic rocks, the intermediate to ultramafic rocks are volumetrically subordinate. The presence of forsteritic olivine and bytownite in some of the ultramafic rocks shows that the magmas from which these crystallized must have been broadly basaltic in composition, whereas the dominance of hornblende throughout the diorites, gabbros and ultramafic rocks indicates that the magmas were either hydrous at the outset or became hydrated through contamination in the crust.

The preservation of stable olivine crystals within hornblende oikocrysts in the olivine hornblendites suggests that hornblende growth must have occurred over a narrow temperature interval (Green, 1982). Compositional differences between the calcic amphiboles of the hornblendites and the olivine hornblendites indicate

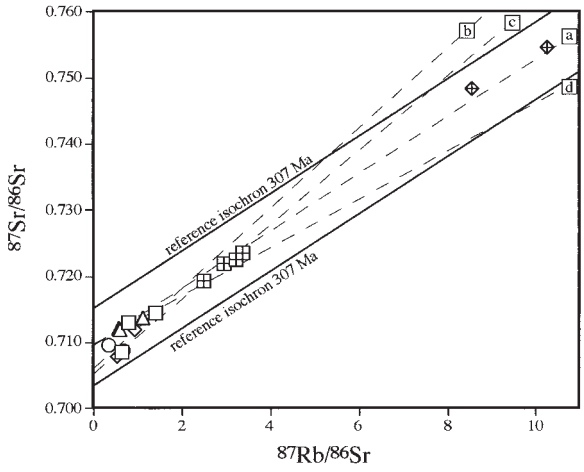


| Line | Data set | Age | MSWD | Initial ratio |
|---|---|---|---|---|
| a | all felsic rocks | 306 ±10 | 41 | 0.7093 ±2 |
| b | all samples | 482 ±83 | 1150 | 0.7061 ±9 |
| c | monzogranites | 397 ±85 | 17 | 0.7053 ±3 |
| d | granodiorites and tonalites | 256 ±72 | 127 | 0.7098 ±7 |

□ diorites △ granodiorites and tonalites
○ hornblende gabbros ⊞ monzogranites
◇ Ol hornblendites ⊕ biotite granite

**Fig. 15.** Plot of $^{87}Sr/^{86}Sr$ vs $^{87}Rb/^{86}Sr$ for the Quérigut Massif rocks. Isochron fits to the dataset, their errors and mean square weighted deviations (MSWD) were calculated using the ISOCHRON program (Provost, 1990).

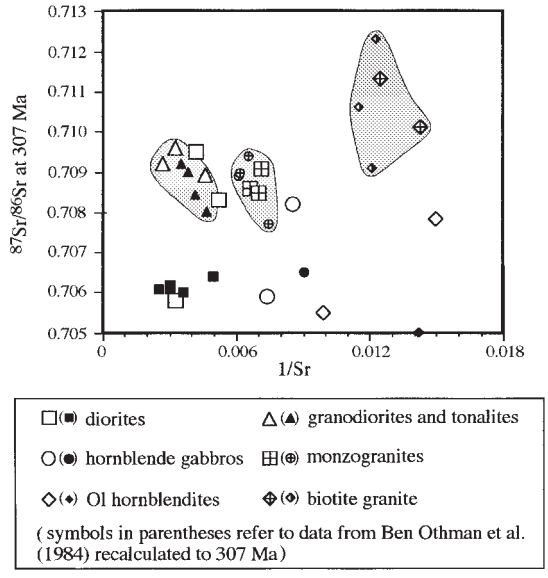


**Fig. 16.** Plot of initial $^{87}Sr/^{86}Sr$ calculated at 307 Ma vs 1/Sr ppm.

that these rocks crystallized from magmas that had different bulk chemistry. Textures in some samples indicate that clinopyroxene and/or orthopyroxene may have been present at one time, but reacted out under sub-solidus conditions forming actinolite (after clinopyroxene) in the hornblendites and cummingtonite (after orthopyroxene) in the olivine hornblendites. Lending some support to this conclusion, Leterrier (1972) reported orthopyroxene in some of his ultramafic rock samples.

The MgO, Cr and Ni contents in the hornblendites and olivine hornblendites are far above those expected for basaltic magmas, which further substantiates a cumulate origin for these rocks, as suggested by Leterrier (1972). The data also indicate that the hornblendites represent cumulates formed from slightly more evolved magmas than those which formed the olivine hornblendites. Although poorly exposed, the common occurrence of these rocks together in the field points to an origin as different levels within layered cumulates formed through fractional crystallization of hydrous mafic magma.

The high Cr content in the hornblende gabbros also indicates that some component of mineral accumulation may have been involved in formation of these rocks. Only the diorites have geochemical compositions that are clearly those of magmatic liquids (Roberts & Clemens, 1995). The occurrence of An-rich plagioclase enclosed by poikilitic hornblende, in the olivine hornblendites and hornblende gabbros, is of particular interest. This texture indicates that the basaltic magmas crystallized at pressures of less than ~300 MPa (Holloway & Burnham, 1972; Green, 1982). Thus, basaltic magma crystallization and cumulate formation occurred in mafic magma chambers at shallow levels in the crust, most probably at the emplacement level of the Massif.

The rimming of bytownite cores by andesine, typical of the diorites and hornblende gabbros, suggests that some kind of magma-mingling process may have operated during magma evolution. Compositions of the rims are broadly similar to those of plagioclase in the granodiorite–tonalite unit, which is the dominant country rock for the intermediate to ultramafic bodies. However, comparison of the Sr isotopic compositions of the hornblende gabbros and diorites with the volume of calcic plagioclase remnant cores present in these rocks (Table 9) reveals that those rocks with the largest volume of andesine have the least evolved Sr isotopic compositions. This is opposite to the expected variation if hybridization was the cause of the core–rim relationship. A possible explanation for this could be an 'incestuous mingling' process, whereby more evolved liquids from the crystallizing mafic–intermediate magmas flux through the interstices of the cumulus mush. Chemical re-equilibration between the liquid and solid could lead to the dissolution of earlier-formed An-rich plagioclase and the precipitation of more sodic rims (i.e. a form of crystal fractionation). Influx of an $H_2O$-rich fluid phase from the crystallizing granitic magma surrounding the mafic intrusions could also have a similar

*Table 8: Sm–Nd isotope composition data of the Quérigut Massif rocks*

| | Sm (ppm) | Nd (ppm) | $^{147}Sm/^{144}Nd$ | $^{143}Nd/^{144}Nd$ | $\varepsilon_{Nd}$ @ 307 Ma | *t*(CHUR) (Ga) | *t*(DM) (Ga) |
|---|---|---|---|---|---|---|---|
| *Diorites* | | | | | | | |
| QM138 | 6·74 | 28·3 | 0·1443 | 0·512389 ± 10 | −2·9 | 0·732 | 1·438 |
| QM197 | 5·93 | 25·4 | 0·1415 | 0·512202 ± 8 | −6·4 | 1·211 | 1·777 |
| QM236 | 4·16 | 18·2 | 0·1380 | 0·512252 ± 10 | −5·3 | 1·009 | 1·594 |
| *Ol hornblendites* | | | | | | | |
| QUM7(1) | 1·28 | 5·65 | 0·1372 | 0·512290 ± 12 | −4·5 | 0·898 | 1·501 |
| QUM71 | 2·29 | 11·5 | 0·1208 | 0·512434 ± 12 | −1·1 | 0·415 | 1·007 |
| *Hornblende gabbros* | | | | | | | |
| QUM119 | 2·80 | 12·0 | 0·1414 | 0·512400 ± 7 | −2·5 | 0·663 | 1·357 |
| QUM144 | 1·20 | 5·70 | 0·1230 | 0·512195 ± 8 | −5·8 | 0·922 | 1·427 |
| *Granodiorite–tonalites* | | | | | | | |
| QH107 | 2·46 | 14·4 | 0·1032 | 0·512175 ± 6 | −5·4 | 0·759 | 1·201 |
| QH170 | 6·35 | 34·8 | 0·1104 | 0·512181 ± 10 | −5·6 | 0·812 | 1·275 |
| QH214 | 4·31 | 28·2 | 0·0925 | 0·512143 ± 10 | −5·6 | 0·728 | 1·137 |
| *Monzogranites* | | | | | | | |
| QH13 | 5·90 | 34·5 | 0·1037 | 0·512167 ± 7 | −5·6 | 0·777 | 1·218 |
| QH35 | 5·00 | 22·4 | 0·1351 | 0·512241 ± 7 | −5·4 | 0·983 | 1·528 |
| QH239 | 4·73 | 28·7 | 0·0996 | 0·512158 ± 10 | −5·6 | 0·758 | 1·187 |
| QH241 | 7·36 | 45·9 | 0·0969 | 0·512166 ± 6 | −5·4 | 0·725 | 1·149 |
| *Biotite granites* | | | | | | | |
| QH89 | 4·90 | 21·9 | 0·1354 | 0·512239 ± 7 | −5·4 | 0·999 | 1·566 |
| QH127 | 4·77 | 19·9 | 0·1449 | 0·512234 ± 10 | −5·9 | 1·196 | 1·794 |

During the course of the analyses, the La Jolla international standard gave $^{143}Nd/^{144}Nd = 0{\cdot}511856 \pm 0{\cdot}000007$ (2σ) for 20 measurements. The raw data were treated using the decay constant recommended by Wasserburg *et al.* (1981). Depleted mantle (DM), chondritic uniform reservoir (CHUR) model ages and $\varepsilon_{Nd}$ values were calculated using the Sm–Nd isotope ratios recommended by DePaolo (1981*b*) for DM, and Jacobsen & Wasserburg (1980) for CHUR and $\varepsilon_{Nd}$. Errors are quoted at 2σ level.

effect. An increase in magma water content would shift the plagioclase liquidus surface to a lower temperature (Dixon & Rutherford, 1983) leading to dissolution of pre-existing An-rich plagioclase. New growth of more sodic plagioclase would then recommence after cooling. What is clear is that this zoning texture in the plagioclase crystals is not unequivocal evidence for magma-mingling. In the hornblende gabbros, the timing of plagioclase dissolution and reprecipitation post-dates the onset of widespread hornblende crystallization, as only An-rich plagioclase is enclosed in hornblende crystals.

Overall, the data (particularly the wide range of Sr–Nd isotope compositions) suggest diverse origins for the diorites. Whereas some diorites show textural evidence for the prior existence of clinopyroxene, other diorite magmas appear to have been hydrous enough to suppress pyroxene crystallization in favour of amphibole from the outset. As suggested above, some diorites may represent comagmatic liquids from closed-system fractionation of mafic magmas involved in the formation of the ultramafic cumulates. This may be the case for those diorites with Sr and Nd isotopes similar to those of the gabbros and ultramafic rocks. Others, particularly samples with Sr and Nd isotope compositions similar to the granodiorite–tonalite rocks, although appearing superficially as hybrids between mafic and granodiorite–tonalite magmas, would seem to represent separate magmas. Alternatively, some of these diorites could be comagmatic with the granodiorite–tonalites either representing early-formed crystal cumulates from the evolving felsic magma, or as parental magmas.

The evolved Sr and Nd isotope signatures of the intermediate to ultramafic rocks and their wide dispersion preclude an origin from a depleted mantle source, unless contamination can be unequivocally demonstrated. However, the exact nature of the mantle underlying the Pyrenees during the Palaeozoic is unknown, which prevents any firm conclusions being drawn from geochemical

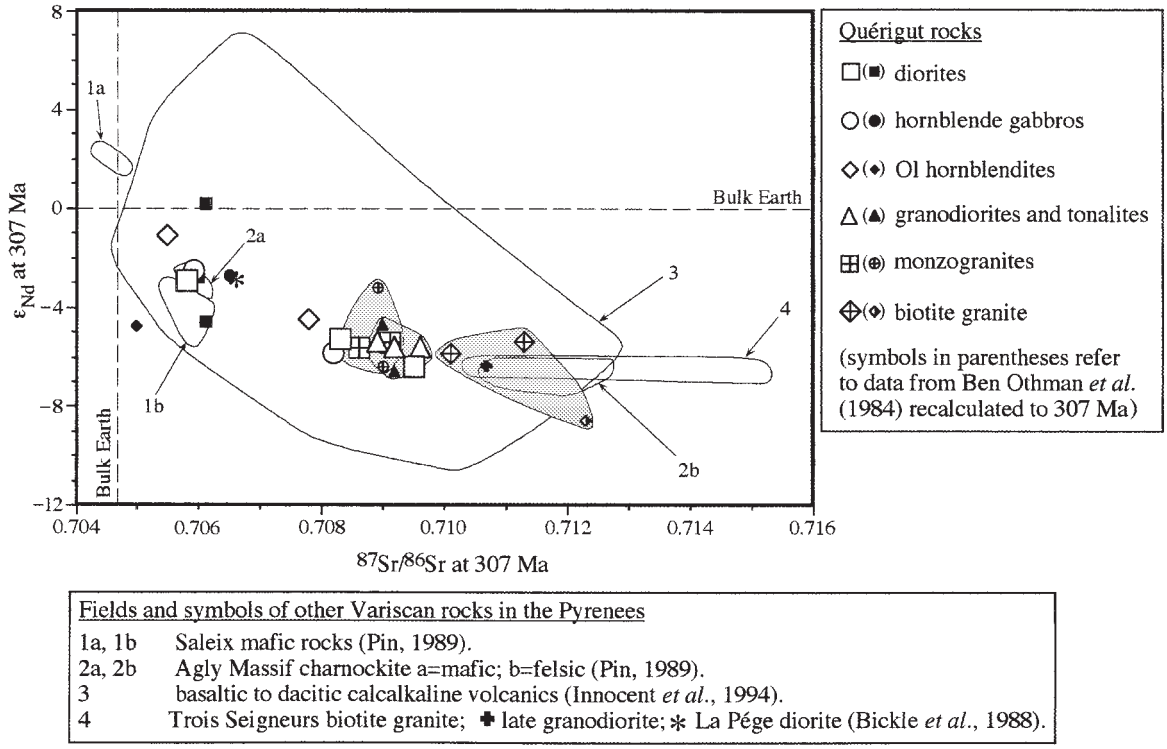


**Fig. 17.** Plot of $\varepsilon_{Nd}$ vs initial $^{87}Sr/^{86}Sr$ ratio both calculated at 307 Ma. Nd and Sr isotope values for other Variscan rocks in the Pyrenees also calculated at 307 Ma.

*Table 9: Comparison of the volume of calcic remnant cores in plagioclase with initial $^{87}Sr/^{86}Sr$ ratio*

| | vol. % calcic remnant cores to bulk plagioclase content* | $^{87}Sr/^{86}Sr$ @ 307 Ma |
|---|---|---|
| *Hornblende gabbro* | | |
| QUM119 | <10% | 0·7059 |
| QUM144 | ~25–30% | 0·7082 |
| *Diorite* | | |
| QM138 | ~10% | 0·7058 |
| QM197 | ~25% | 0·7095 |
| QM236 | ~25% | 0·7083 |

*Proportion of the total plagioclase content of each rock represented by calcic ($An_{70–90}$) cores. The remainder of the plagioclase component has a composition of $An_{40–60}$.

modelling, because it is impossible to constrain the composition of the mafic end-member, although determined as being broadly a high-Al basalt (Leterrier, 1972). On the basis of geochemical and isotopic data for deep-seated Saleix mafic intrusions, it has been suggested that the mantle beneath the Pyrenees was heterogeneous, with both enriched and depleted domains, as is typical for subcontinental regions (Pin, 1989). The occurrence of an enriched domain in the underlying mantle comes also from the low $\varepsilon_{Nd}$ at 307 Ma value (–4·8) of ultramafic rock sample Qt46 (Table 10). As discussed by Ben Othman *et al.* (1984), low Nd contents of the ultramafic cumulates make them susceptible to post-crystallization contamination. This effect could well be magnified in a geochemically and isotopically labile (reactive) environment, such as a crystallizing and evolving granitic magma body. However, Qt46 also has a mantle-like $\delta^{18}O$ value (+5·8) that does not support contamination or late-stage alteration, evidence of which is absent from the brief petrographic description of this sample [see appendix of Fourcade & Allègre (1981)]. Thus, the wide spread of the isotopic data for the intermediate to ultramafic rocks may simply reflect a heterogeneous mantle.

Areal extents and rock textures indicate that small volumes of intermediate and mafic magmas were able to ascend to shallow levels in the Pyrenean crust. These probably intruded contemporaneously with the granitoid magmas, and formed magma chambers within which crystal fractionation and accumulation occurred. Ascent

*Table 10: Compilation of the available isotopic data for the Quérigut Massif*

| | Previously published data* | | | This study | | | Data range | | |
|---|---|---|---|---|---|---|---|---|---|
| | $^{87}Sr/^{86}Sr$† | $\varepsilon_{Nd}$† | $\delta^{18}O$ | | $^{87}Sr/^{86}Sr$† | $\varepsilon_{Nd}$† | $^{87}Sr/^{86}Sr$† | $\varepsilon_{Nd}$† | $\delta^{18}O$ |
| *Olivine hornblendite* | | | | | | | | | |
| Qt46 | 0·7050 | −4·8 | 5·75 | QUM7(1) | 0·7078 | −4·5 | 0·7050–0·7078 | −1·1 to −4·8 | 5·75 |
| | | | | QUM71 | 0·7055 | −1·1 | | | |
| *Hornblende gabbro* | | | | | | | | | |
| Qt104 | 0·7065 | −2·7 | 6·1 | QM119 | 0·7059 | −2·5 | 0·7059–0·7082 | −2·5 to −5·8 | 6·1 |
| | | | | QM144 | 0·7082 | −5·8 | | | |
| *Diorites* | | | | | | | | | |
| Qt02 | 0·7078 | — | 8·25 | QM138 | 0·7058 | −2·9 | 0·7058–0·7095 | +0·2 to −6·4 | 7·15–8·25 |
| Qt04 | 0·7064 | — | 7·3 | QM197 | 0·7095 | −6·4 | | | |
| Qt07 | 0·7061 | −4·6 | 8·05 | QM236 | 0·7083 | −5·3 | | | |
| Qt08 | 0·7061 | +0·2 | 7·5 | | | | | | |
| Qt09 | — | — | 7·2 | | | | | | |
| Qt10 | 0·7060 | −2·8 | 7·15 | | | | | | |
| Qt44 | — | — | 8·0 | | | | | | |
| *Granodiorite–tonalites* | | | | | | | | | |
| Qt25 | 0·7092 | −6·6 | 8·95 | QH107 | 0·7089 | −5·4 | 0·7089–0·7096 | −4·7 to −6·6 | 8·6 to 9·4 |
| Qt40 | 0·7090 | — | 8·6 | QH214 | 0·7096 | −5·6 | | | |
| Qt45 | — | — | 9·25 | QH170 | 0·7092 | −5·6 | | | |
| Qt52 | 0·7090 | −4·7 | 9·4 | | | | | | |
| *Monzogranites* | | | | | | | | | |
| Qt12 | 0·7089 | −3·2 | 9·15 | QH239 | 0·7085 | −5·6 | 0·7085–0·7091 | −3·2 to −6·4 | 9·15 to 9·8 |
| Qt13 | — | — | 9·5 | QH241 | 0·7091 | −5·4 | | | |
| Qt18 | 0·7090 | −6·4 | 9·65 | QH35 | 0·7091 | −5·6 | | | |
| Qt43 | — | — | 9·8 | QH13 | 0·7086 | −5·4 | | | |
| Qt51 | — | — | 9·5 | | | | | | |
| Qt83 | — | — | 9·65 | | | | | | |
| *Biotite granites* | | | | | | | | | |
| Qt15 | 0·7123 | −8·6 | 10·2 | QH127 | 0·7101 | −5·4 | 0·7092–0·7123 | −5·4 to −8·6 | 10·2 to 10·6 |
| Qt31 | — | −6·7 | 10·25 | QH89 | 0·7113 | −5·9 | | | |
| Qt32 | 0·7092 | — | 10·25 | | | | | | |
| Qt33 | 0·7107 | — | 10·6 | | | | | | |

*Data taken from Ben Othman *et al.* (1984) and Fourcade & Javoy (1991).
†All isotopic ratios and $\varepsilon_{Nd}$ values calculated at 307 Ma.

to the upper-crustal emplacement level may have been facilitated by shear zones such as the Mérens Fault. This structure shows evidence in the granodiorite–tonalite unit for having been active during emplacement of the Massif (Roberts, 1994) and probably acted as one of a number of potential pathways along which mantle-derived magma could be tapped and transferred to the upper crust. Similar mafic–felsic complexes in other parts of the Variscan orogenic belt may also owe their existence to the proximity of crustal shear zones [see data of Dias & Leterrier (1994) and Galán *et al.* (1996)].

## Felsic series

The dominant components of the Massif are the granitoids. These are mineralogically and chemically metaluminous to weakly peraluminous. Major element

variations show that they are calc-alkaline to high-K calc-alkaline, I-types, suggesting a role for meta-igneous material in the formation of the Quérigut magmas. In terms of their respective mineralogies, the granodiorite–tonalite, monzogranite and biotite granite units show distinct differences. Broadly, the mafic minerals become more Fe rich with increasing $SiO_2$ content of the magmas. Biotite is markedly more aluminous in the biotite granite compared with the granodiorite–tonalite and monzogranite. The presence of hornblende in the granodiorite–tonalite and monzogranite units suggests magma water contents of $\geq 4$ wt % (Naney, 1983). The presence of magmatic epidote was commonly considered as evidence for magma crystallization at pressures >800 MPa (Zen & Hammarstrom, 1984). However, recent experiments (Roberts & Clemens, 1994; Schmidt & Thompson, 1996) have shown that it is stable above the solidus in tonalitic to granodioritic magmas down to pressures as low as 400 MPa. Hence, it is of little use as a pressure indicator, although the aforementioned experimental studies do show that the low-pressure crystallization of magmatic epidote indicates high $fO_2$.

Similarities in the Sr, Nd and O isotope signatures of the granodiorite–tonalite and monzogranite units indicate that they could be petrogenetically related through closed-system crystal fractionation. This is highlighted in Fig. 16, which shows that the granodiorite–tonalite unit is offset towards higher Sr contents compared with the monzogranite at the same initial $^{87}Sr/^{86}Sr$ ratio. This indicates that the granodiorite–tonalite rocks may be related to the monzogranite by plagioclase fractionation. However, the CaO, $Al_2O_3$ and Sr contents of the granodiorite–tonalite rocks also appear to be normal for dacitic magmas (Ewart, 1979). On this basis, the granodiorite–tonalite unit could equally well represent a separate, more mafic, granitoid magma derived from a source with time-integrated Rb/Sr and Sm/Nd ratios similar to those of the monzogranite. Unfortunately, $\delta^{18}O$ data compiled in Table 10 favour neither of the models. The slightly lower $\delta^{18}O$ values for the granodiorite–tonalite unit compared with the monzogranite could simply reflect the different modal abundances of their constituent minerals [see full $\delta^{18}O$ dataset of Fourcade & Javoy (1991)].

The geochemical variability between samples of the granodiorite–tonalite unit, notably $SiO_2$, CaO, $Al_2O_3$ and Sr, indicates that this magma body is compositionally diverse, despite being isotopically homogeneous. Some foliated granodiorite–tonalite samples collected near the southern margin of the pluton show evidence for subsolidus recrystallization and extreme elongation of enclaves (Roberts, 1994), and have distinctly lower $SiO_2$ and higher $Al_2O_3$ contents, and slightly more mafic compositions compared with unfoliated samples. These rocks could have assumed the compositions of plagioclase cumulates through the expressing of melt during simultaneous crystallization and shearing. The chemical variability among other samples of granodiorite–tonalite rocks could reflect differing degrees of mineral accumulation during closed-system fractionation.

Some aspects of the chemical variation between the biotite granite and the monzogranite could be interpreted as evidence for a comagmatic linkage between these units. However, there are important differences, such as the higher Rb contents and much higher Rb/Sr ratios, that preclude such an interpretation. Also, in terms of its Sr and Nd isotope compositions, the biotite granite unit has a more crustal signature than both the granodiorite–tonalite and the monzogranite units. The $\delta^{18}O$ values for this unit (Table 10) are also more crustal than those of the granodiorite–tonalite and monzogranite units (Fourcade & Javoy, 1991). Taken together, this suggests that the protolith for the biotite granite unit was more crustally evolved and distinct from that of the other felsic rocks.

## Petrogenetic model

The postulated petrogenetic relationships between the Quérigut rocks are summarized in Fig. 19. Mineralogical and geochemical data indicate that the protoliths for the granitic rocks were essentially of igneous origin. Radiogenic isotope data highlight the considerable crustal residence age of the source region and show that the granitoid magmas do not represent new additions to the crust. Possible protoliths could be ancient volcanogenic rocks in the lower crust, and consisting, at the time of magma genesis, of amphibolitized calc-alkaline to high-K calc-alkaline basaltic andesites and andesitic metagreywackes (Roberts & Clemens, 1993).

On the basis of Sr, Nd and O isotope variation (Figs 17 and 18), it would seem feasible that the granitic magmas were formed by variable degrees of mixing between mafic magmas and partial melts derived from older metasedimentary components (with high initial $^{87}Sr/^{86}Sr$, low $\varepsilon_{Ndi}$ and high $\delta^{18}O$) in the lower crust, with the crustal component clearly dominant. The lack of chemical and isotopic suitability of the common Pyrenean pelitic rocks as sources has already been discussed (Bickle *et al.*, 1988; Roberts & Clemens, 1995). In either a mixing or a separate source model for the granitoid magmatism, the protoliths probably contained variable amounts of a recycled crustal component that had been subjected to surficial weathering as suggested by the $\delta^{18}O$ values (Table 10). Partial melting of the crustal rocks was probably in response to heat input in the form of mantle-derived mafic magmas.

The relatively mafic composition of the granodiorite–tonalite unit relative to the monzogranite unit, coupled

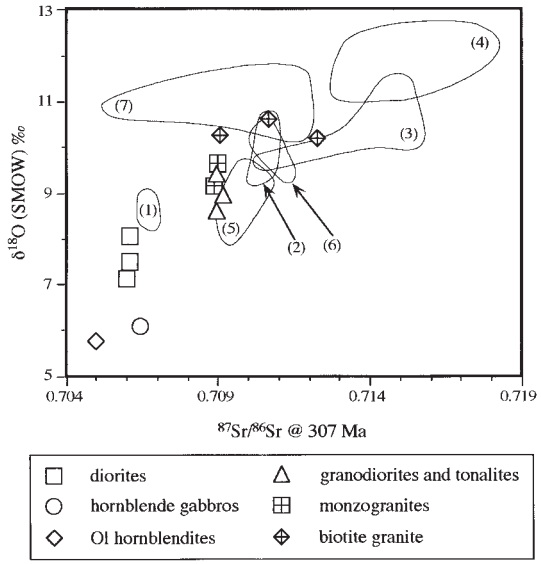


**Fig. 18.** Plot of $\delta^{18}O$ (SMOW) vs initial $^{87}Sr/^{86}Sr$ at 307 Ma. Data for the Quérigut rocks taken from Fourcade & Javoy (1991). Fields of other Variscan rocks in the Pyrenees are: (1) La Pége diorite (Trois Seigneurs Massif); (2) Trois Seigneurs late granodiorite; (3) Trois Seigneurs biotite granite; (4) Trois Seigneurs regional pelitic schists; (5) Maladeta Massif mafic rocks; (6) Maladeta Massif granodiorite; (7) Maladeta Massif two-mica cordierite granite. 1–4, from Bickle *et al.* (1988); 5–7, from Michard-Vitrac *et al.* (1980).

with similar isotope signatures, suggests that they may have been derived either from similar protoliths (model 1 in Fig. 19) or that the granodiorite–tonalite unit represents a cumulate from the magma that also formed the monzogranite (model 2 in Fig. 19). The available evidence suggests that both models are feasible. Petrological, geochemical and isotopic data clearly show that the biotite granite represents a separate magma batch that, because of the sharp contacts with the then solid surrounding monzogranite, was most probably the final magma addition to the Massif.

The common association of the granodiorite–tonalite unit with intermediate and mafic rocks, as large masses typically surrounded by magmatic diorite enclaves (Leterrier & Debon, 1978; Fourcade & Javoy, 1991) suggests that these felsic and mafic magmas were emplaced contemporaneously. The mafic magmas built up small magma chambers within the granodiorite–tonalite unit, and rarely the monzogranite unit, where they underwent fractional crystallization forming the diorites, hornblende gabbros and layered ultramafic hornblendite and olivine hornblendite cumulates. Some diorites may be crystal cumulates from the granodiorites and tonalites.

Although there is abundant evidence for magma mingling in the Quérigut Massif, magma mixing during ascent and emplacement appears to have been of little importance. There is considerable overlap in the initial isotope

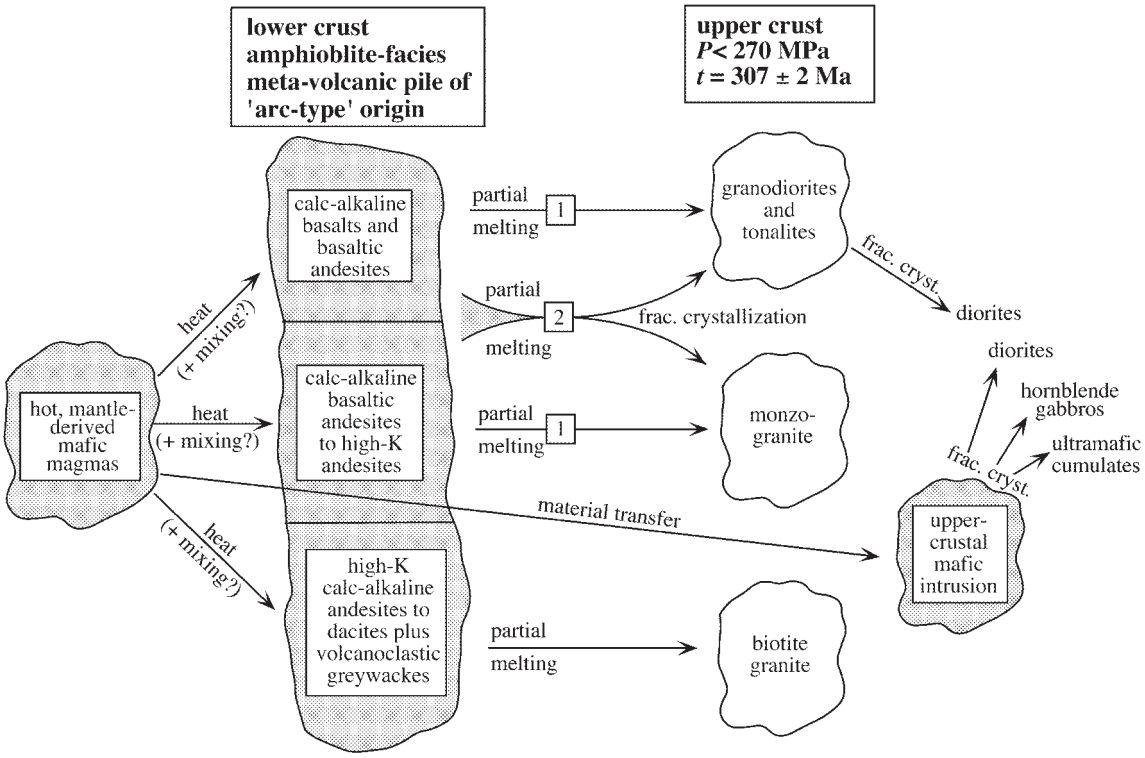


**Fig. 19.** Petrogenetic model for the evolution of the Quérigut Massif.

ratios for the suite (Table 10), and a distinctly chaotic nature in the distribution of the values among the rocks, which is not as might be expected in the case of magma mixing. Geochemical and petrographic data suggest that it was the rocks or magmas of the mafic series that underwent limited hybridization with crustal materials (alkalis, radiogenic Sr and Nd, $H_2O$). The effects of this are particularly noticeable from the isotopic data in Table 10, where there is a general lack of accord between Sr, Nd and O isotopes from the dataset of Ben Othman *et al.* (1984) and Fourcade & Javoy (1991) obtained mostly from the same intermediate to ultramafic body. The presence of cummingtonite and actinolite in some gabbros and the ultramafic rocks indicates sub-solidus reaction with a late magmatic fluid phase, most probably derived from the felsic rocks during cooling.

In agreement with Fourcade & Allègre (1981) and Fourcade & Javoy (1991), we suggest that mantle-derived mafic magmas played an important part in the formation of the Quérigut granitoid suite. However, there is little evidence that these played a material role beyond acting as a heat source to promote partial melting in the crust. Contrary to the opinion of Ben Othman *et al.* (1984), we believe that the intermediate to mafic magmas emplaced contemporaneously with the Quérigut granitoids are not those that lead to partial melting, although they were probably broadly cogenetic. Textures shown by these rocks indicate that crystallization of the magmas occurred at the emplacement level rather than at depth, as would be expected for mafic magmas losing heat to the lower-crustal protoliths during partial melting. However, it is possible that some of the intermediate magmas represent evolved liquids from the lower-crustal mafic magmas that acted as a heat source.

The dispersion of Sr and Nd isotope data for Variscan magmatic and high-grade metamorphic rocks in the Pyrenees (Fig. 17) highlights the wide diversity of materials involved in this episode of crustal differentiation, which hinders the task of identifying any potential mantle or crustal end-members if mixing were the cause of the variation. This diversity is particularly apparent for the calc-alkaline volcanic rocks (Innocent *et al.*, 1994), the Sr and Nd isotopic compositions of which cover virtually the whole spectrum shown by all the other data.

An interesting feature is the similarity of the Quérigut Massif biotite granite (Figs 17 and 18) to the late granodiorite of the Trois Seigneurs Massif (Bickle *et al.*, 1988), which indicates that the materials involved in magma genesis are not a local occurrence. The Nd, Sr and O isotopic compositions of the Agly Massif felsic charnockite (Pin, 1989) are also similar to those of the Quérigut biotite granite. These granulites are peraluminous, associated with mafic magmas with depleted mantle Nd isotopes, and thought to represent fragments of the Variscan lower crust in the Pyrenees (e.g. Guitard *et al.*, 1998). Their peraluminous (S-type) composition and similarity in time-integrated Sr and Nd isotopes to the (I-type) Quérigut biotite granite rules out their suitability as a crustal end-member for magma-mixing. Likewise, for the granodiorite–tonalite and monzogranite units to be products of mixing between mantle mafic magma and a peraluminous felsic partial melt similar in composition to the felsic granulites, greater variation in Sr and Nd isotopic composition would be expected considering the differences in geochemistry of these two units. It should be noted in Fig. 17 that the monzogranites have marginally lower $^{87}Sr/^{86}Sr$ and higher $\varepsilon_{Nd}$ at 307 Ma than the granodiorite–tonalite unit, which is the reverse of the variation expected from mixing.

Petrogenetic evolution of the Maladeta Massif would appear to have been similar to that of the Quérigut Massif, although the data require a greater contribution from evolved sedimentary material coupled with an enriched mantle domain in the former case. Mantle material input in the formation of the Trois Seigneurs Massif would also appear to have been similar to the Quérigut Massif in terms of Sr, Nd and O isotopic composition. In contrast to the felsic suite of Quérigut, that of the Maladeta Massif requires a strongly peraluminous protolith for formation of the two-mica cordierite granite (Michard-Vitrac *et al.*, 1980). Unfortunately, no Sm–Nd isotope data are published for the Maladeta rocks to assess their differences from or similarities to the peraluminous granulites, although comparison of their initial $^{87}Sr/^{86}Sr$ at 307 Ma (Fig. 18) does suggest that the material from which the granulites were derived could also represent suitable protoliths for the Maladeta two-mica granites.

The protoliths envisaged as sources for the Quérigut granitoids (i.e. calc-alkaline, metaluminous rocks) appear to be exotic in terms of Pyrenean geology, as they do not crop out at the present level of exposure of the mountain chain. In the case where a lower-crustal mixing origin for the granitic rocks is favoured, it should be pointed out that there is no evidence for mafic–felsic hybridization in association with the small exposed slices of granulites in the North Pyrenean Massifs, or that these granulites represent, or are representative of, the lower crust in the Pyrenean area [compare, for example, Guitard *et al.* (1998)].

## Tectonic setting of Pyrenean epizonal magmatism

The tectonic setting of Variscan orogenesis in the Pyrenees is controversial, with hypotheses involving collision (e.g. Matte, 1986; Matte & Mattauer, 1987) or extension (e.g. Wickham & Oxburgh, 1985) being proffered. Generally, published models for the tectonic history of the European Variscides do not focus on the Pyrenean Axial

Zone (e.g. Franke, 1989; Pin, 1989), not only because of the complexities that have arisen through the diachronous nature of metamorphism and deformation (Banda & Wickham, 1986), but also because this region forms a small, relatively external part of the Variscan belt.

In terms of their structural position within the Variscan belt, the Pyrenees are part of the external zone along the southern flank of the orogen (Arthaud & Matte, 1977*a*). The sedimentary record shows that nappe tectonics in the external zones ended with deposition of flysch sequences, including olistostromes, during the mid-Westphalian (Engel & Franke, 1983). The widespread HT–LP metamorphism, with almost no mineralogical trace of a high-pressure event (e.g. Vielzeuf, 1980, 1984; Andrieux, 1982; Zwart, 1986; Guitard *et al.*, 1998), suggests that the collisional phase of the Variscan orogeny did not involve major crustal thickening in the external zones. On the contrary, the high heat flow probably indicates the crust was thin at this stage.

Following crustal shortening, a wrench-dominated tectonic regime led to the development of pull-apart basins, and the deposition of terrestrial red-bed sequences dated as Stephanian (Arthaud & Matte, 1977*b*). Extension and basin formation persisted through into the Permian (Vissers, 1992), with the basins acting as loci for the emplacement of the granitoid complexes and eruption of calc-alkaline volcanic rocks (Briqueu & Innocent, 1993; Gilbert *et al.*, 1994; Innocent *et al.*, 1994). Formation of mafic magmas and lower-crustal anatexis may have been associated with the detachment of a cold gravitationally unstable lithospheric root (Pin, 1989; Vissers, 1992).

At variance with the tectonic model proposed by Innocent *et al.* (1994), we believe that post-collisional wrenching (in the external zones) was well under way by at least 310 Ma (Westphalian). This corresponds to the early Permian 275 Ma rifting event of Innocent *et al.* (1994). This point in geological time is also characterized by a major change in sedimentation style associated with a change from marine to terrestrial conditions. Recently published U–Pb ages on other Pyrenean high-level granitoid complexes (Romer & Soler, 1995; Paquette *et al.*, 1997) suggest that it was during the late Carboniferous transpression–transtension phase that the granitoid magmas were formed and emplaced.

Recent structural studies have suggested that the Pyrenean high-level granitoids are 'syn-tectonic' and emplaced during a compressional phase (Gleizes *et al.*, 1997; Evans *et al.*, 1998). However, whether it is reasonable to relate the local structures formed through emplacement to the overall tectonic regime prevailing at the time of magma intrusion is questionable. Clearly, the widespread occurrence of mafic rocks within many of the upper-crustal granitoids of the Pyrenees (e.g. Michard-Vitrac *et al.*,1980) calls for an element of mantle decompression, most efficiently facilitated by extension, whatever its cause.

Much of the so-called extensional phase of the Variscan orogen in the Pyrenean area appears to have involved a long history of movement along major strike-slip faults during the juxtaposition of the Iberian and European plates (Arthaud & Matte, 1977*b*; Matte, 1986; Matte & Mattauer, 1987). The situation contrasts with simple gravitational collapse of a tectonically thickened crust. Indeed, there is no clear evidence for the existence of any such thickened crust. In this sense, the late-orogenic granitoids in the Pyrenean area are 'anomalous', as they do not fit the commonly accepted model for post-collisional magmatism (Pitcher, 1987). However, calc-alkaline granitoids do occur in other tectonic settings, such as continental arcs and their margins (e.g. Andes; Pitcher, 1987; Atherton, 1990) or in intracontinental rifts (e.g. Lachlan fold belt, SE Australia; Collins & Vernon, 1992; Coney, 1992). In this sense, a unique model to explain their occurrence and distribution is clearly inadequate. Attention should also be paid to the broad regional geology and its causes rather than focusing on the geochemical and isotopic characteristics of the granitoids in isolation.

## CONCLUSION

The available data indicate that Variscan magmatism in the Pyrenees involved the reworking of a heterogeneous crustal pile consisting of older meta-igneous and volcanosedimentary material in response to heat and material input from a heterogeneous mantle domain. The data do not support simple mixing or AFC-type processes involving mafic mantle and peraluminous crustal end-members. This highlights the potential of granitoid rocks to act as windows through which the composition of the lower crust may be viewed. Although the final solidified rocks are unlikely to mirror faithfully the source region from which they were initially extracted, granitoid rocks permit indirect constraints to be placed on the previous geological history of an area for which there may be no surface expression.

This study reinforces the fact that extreme care is needed in the interpretation of geochemical and isotopic data. All potential models should be sought and evaluated. Clearly, the petrogenetic relations involved in crustal magmatism (such as in the Quérigut Massif) can be extremely complex. Thus, in pursuit of a model to explain the formation of a given granitic magma, the question arises of whether a mixing-type model, which relies on complex and poorly understood physicochemical processes, is a more realistic choice than a model involving multiple independent sources. In a situation where the data are equivocal, the final choice appears, at present,

to be based on personal preference. It is surely unreasonable to conclude that the very limited exposures of the lower crust in a mountain chain such as the Pyrenees are representative of the composition of the lower crust in the entire region. Both the lower crust and the upper mantle are generally highly heterogeneous. As geologists are generally pragmatists, there is very often a tendency to opt for a model involving materials that are known to be present (exposed) in a region, rather than a model involving materials that might be present (unexposed) at depth. Such a decision could have the effect that intriguing and important possibilities remain untested.

## ACKNOWLEDGEMENTS

The authors would like to thank Chantal Bassin (Clermont-Ferrand) for her assistance with the Rb–Sr analyses, and Dave Plant and Tim Hopkins (Manchester) for their help with the electron microprobe. This work was partially funded through an NERC post-graduate research studentship to M.P.R. at Manchester University. Constructive reviews from Daniel Vielzeuf and Steve Wickham helped immensely in ironing out ambiguities.

## REFERENCES

Althaus, E., Karotke, E., Nitsch, K. H. & Winkler, H. G. F. (1970). An experimental re-examination of the upper stability limit of muscovite plus quartz. *Neues Jahrbuch für Mineralogie, Monatshefte* **7**, 325–336.

Andrieux, P. (1982). La charnockite d'Ansignan (Massif d'Agly, Pyrénées Orientales). Mise en place et évolution paragénétique. Introduction à l'étude des équilibres grenat–orthopyroxÈne. 3rd Cycle Thesis, Université Blaise Pascal, Clermont-Ferrand, 109 pp.

Aparicio, M. (1975). Métamorphisme et déformation au contact d'un massif plutonique, l'encaissent du complexe de Quérigut. 3rd Cycle Thesis, Université Paul Sabatier, Toulouse.

Aparicio, M. (1977). Relations entre la déformation et le métamorphisme dans les skarns de l'auréole de contact du complexe éruptif de Quérigut (Pyrénées Orientales). *Comptes Rendus de l'Académie des Sciences, Série D* **284**, 1753–1756.

Arthaud, F. & Matte, P. (1977*a*). SynthÈse provisoire sur l'évolution tectonique et les raccords entre les segments Hercyniens situes autour du bassin Nord-Balaere (sud de la France, Espagne, bloc Corso-Sarde). *Colloquium International du CNRS, Rennes* **243**, 497–513.

Arthaud, F. & Matte, P. (1977*b*). Late Paleozoic strike-slip faulting in southern Europe and northern Africa: result of a right-lateral shear zone between the Appalachians and the Urals. *Geological Society of America Bulletin* **88**, 1305–1320.

Atherton, M. P. (1990). The Coastal Batholith of Peru: the product of rapid recycling of 'new' crust formed within rifted continental margin. *Geological Journal* **25**, 337–349.

Banda, E. & Wickham, S. M. (1986). The geological evolution of the Pyrenees—an introduction. *Tectonophysics* **129**, 1–7.

Barker, F., Wones, D. R., Sharp, W. N. & Desborough, G. A. (1975). The Pikes Peak batholith, Colorado Front Range, and a model for the origin of the gabbro–anorthosite–syenite–potassic granite suite. *Precambrian Research* **3**, 97–160.

Beckinsale, R. D., Sanchez-Fernandez, A. W., Brook, M., Cobbing, E. J., Taylor, W. P. & Moore, N. D. (1985). Rb–Sr whole rock isochron and K–Ar age determinations for the Coastal Batholith of Peru. In: Pitcher, W. S., Atherton, M. P., Cobbing, E. J. & Beckinsale, R. D. (eds) *Magmatism at the Plate Edge—the Peruvian Andes*. Glasgow: Blackie, pp. 177–202.

Ben Othman, D., Fourcade, S. & Allègre, C. J. (1984). Recycling processes in granite–granodiorite genesis: the Quérigut case studied by Nd–Sr isotope systematics. *Earth and Planetary Science Letters* **69**, 290–300.

Bickle, M. J., Wickham, S. M., Chapman, H. J. & Taylor, J. H. P. (1988). A strontium, neodymium and oxygen isotope study of hydrothermal metamorphism and crustal anatexis in the Trois Seigneurs Massif, Pyrenees, France. *Contributions to Mineralogy and Petrology* **100**, 399–417.

Briqueu, L. & Innocent, C. (1993). Datation U/Pb sur zircon et géochimie isotopique Sr et Nd du volcanisme Permien des Pyrénées occidentales (Ossau et Anayet). *Comptes Rendus de l'Académie des Sciences, Série II* **316**, 623–628.

Brophy, J. G. (1991). Composition gaps, critical crystallinity, and fractional crystallisation in orogenic (calc-alkaline) magmatic systems. *Contributions to Mineralogy and Petrology* **109**, 173–182.

Brown, G. C., Hughes, D. J. & Esson, J. (1973). New X.R.F. data retrieval techniques and their application to U.S.G.S. standard rocks. *Chemical Geology* **11**, 223–229.

Cawthorn, R. G. (1976). Some chemical controls on igneous amphibole compositions. *Geochimica et Cosmochimica Acta* **40**, 1319–1328.

Chappell, B. W. (1996). Magma mixing and the production of compositional variation within granite suites: evidence from the granites of Southeastern Australia. *Journal of Petrology* **37**, 449–470.

Chappell, B. W. & White, A. J. R. (1974). Two contrasting granite types. *Pacific Geology* **8**, 173–174.

Chappell, B. W., White, A. J. R. & Wyborn, D. (1987). The importance of residual source material (restite) in granite petrogenesis. *Journal of Petrology* **28**, 1111–1138.

Chatterjee, N. D. & Froese, E. (1975). A thermodynamic study of the pseudobinary join muscovite–paragonite in the system $KAlSi_3O_8$–$NaAlSi_3O_8$–$Al_2O_3$–$SiO_2$–$H_2O$. *American Mineralogist* **60**, 985–993.

Clarke, D. B. (1992). *Granitoid Rocks*. London: Chapman & Hall, 283 pp.

Clemens, J. D. (1984). Water contents of silicic to intermediate magmas. *Lithos* **17**, 275–287.

Clemens, J. D. (1990). The granulite–granite connexion. In: Vielzeuf, D. & Vidal, P. (eds) *Granulites and Crustal Evolution*. Dordrecht: Kluwer Academic, pp. 25–36.

Clemens, J. D. & Droop, G. T. R. (1998). Fluids, *P–T* paths and the fates of anatectic melts in the Earth's crust. *Lithos* **44**, 21–36.

Clemens, J. D. & Mawer, C. K. (1992). Magma transport by fracture propagation. *Tectonophysics* **204**, 339–360.

Collins, W. J. & Vernon, R. H. (1992). Palaeozoic arc growth, deformation and migration across the Lachlan Fold Belt, south-eastern Australia. *Tectonophysics* **214**, 381–400.

Coney, P. J. (1992). The Lachlan belt of eastern Australia and circum-Pacific tectonic evolution. *Tectonophysics* **214**, 1–25.

DePaolo, D. J. (1981*a*). Trace element and isotopic effects of combined wallrock assimilation and fractional crystallisation. *Earth and Planetary Science Letters* **53**, 189–202.

DePaolo, D. J. (1981*b*). Neodymium isotopes in the Colorado Front range and crust–mantle evolution in the Proterozoic. *Nature* **298**, 193–196.

DePaolo, D. J., Perry, F. V. & Baldridge, W. S. (1992). Crustal versus mantle sources of granitic magmas: a two-parameter model based on Nd isotopic studies. *Philosophical Transactions of the Royal Society, Edinburgh* **83**, 439–446.

Dias, G. & Leterrier, J. (1994). The genesis of felsic–mafic plutonic associations: a Sr and Nd isotopic study of the Hercynian Braga Granitoid Massif (Northern Portugal). *Lithos* **32**, 207–223.

Dixon, S. & Rutherford, M. J. (1983). The origin of rhyolite and plagiogranite in oceanic crust: an experimental study. *Journal of Petrology* **24**, 1–25.

Droop, G. T. R. (1987). A general equation for estimating $Fe^{3+}$ concentrations in ferromagnesian silicates and oxides from microprobe analyses, using stoichiometric criteria. *Mineralogical Magazine* **51**, 431–435.

Druitt, T. H. & Bacon, C. R. (1989). Petrology of the zoned calcalkaline magma chamber of Mount Mazama, Crater Lake, Oregon. *Contributions to Mineralogy and Petrology* **101**, 245–259.

Engel, W. & Franke, W. (1983). Flysch-sedimentation: its relations to tectonism in the European Variscides. In: Martin, H. & Eder, F. W. (eds) *Intracontinental Fold Belts*. Berlin: Springer, pp. 289–321.

England, P. C. & Thompson, A. B. (1984). Pressure–temperature–time paths of regional metamorphism, Part 1: Heat transfer during the evolution of regions of thickened continental crust. *Journal of Petrology* **25**, 894–928.

Evans, N. G., Gleizes, G., Leblanc, D. & Bouchez, J. L. (1998). Syntectonic emplacement of the Maladeta granite (Pyrenees) deduced from the relationships between Hercynian deformation and contact metamorphism. *Journal of the Geological Society, London* **155**, 209–216.

Ewart, A. (1979). A review of the mineralogy and chemistry of Tertiary–Recent, dacitic, latitic, rhyolitic and related salic volcanic rocks. In: Barker, F. (ed.) *Developments in Petrology 6, Trondhjemites, Dacites and Related Rocks*. Amsterdam: Elsevier, pp. 13–121.

Fonarev, V. I. & Korolkov, G. Y. (1980). The assemblage orthopyroxene + cummingtonite + quartz. The low-temperature stability limit. *Contributions to Mineralogy and Petrology* **73**, 413–420.

Fourcade, S. & Allègre, C. J. (1981). Trace element behaviour in granite genesis: a case study. The calcalkaline plutonic association from the Quérigut Complex (Pyrenees, France). *Contributions to Mineralogy and Petrology* **76**, 177–195.

Fourcade, S. & Javoy, M. (1991). Sr–Nd–O isotopic features of mafic microgranular enclaves and host granitoids from the Pyrenees, France: evidence for their hybrid nature and inference on their origin. In: Didier, J. & Barbarin, B. (eds) *Enclaves and Granite Petrology*. Amsterdam: Elsevier, pp. 345–365.

Franke, W. (1989). Tectonostratigraphic units in the Variscan belt of central Europe. *Geological Society of America, Special Paper* **230**, 67–87.

Galán, G., Pin, C. & Duthou, J.-L. (1996). Sr–Nd isotopic record of multi-stage interactions between mantle-derived magmas and crustal components in a collision context—the ultramafic–granitoid association from Vivero (Hercynian belt, NW Spain). *Chemical Geology* **131**, 67–91.

Gilbert, J. S., Bickle, M. J. & Chapman, H. J. (1994). The origin of Pyrenean Hercynian volcanic rocks (France–Spain): REE and Sm–Nd isotope constraints. *Chemical Geology* **111**, 207–226.

Gleizes, G., Leblanc, D. & Bouchez, J. L. (1997). Variscan granites of the Pyrenees revisited: their role as syntectonic markers of the orogen. *Terra Nova* **9**, 38–41.

Green, T. H. (1982). Anatexis of mafic crust and high pressure crystallisation of andesite. In: Thorpe, R. S. (ed.) *Andesites: Orogenic Andesites and Related Rocks*. Chichester: John Wiley, pp. 465–487.

Gribble, R. F., Barnes, C. G., Donato, M. M., Hoover, J. D. & Kistler, R. W. (1990). Geochemistry and intrusive history of the Ashland Pluton, Klamath Mountains, California and Oregon. *Journal of Petrology* **31**, 883–923.

Guitard, G., Vielzeuf, D. & Martinez, F. (1998). Le métamorphisme hercynien. In: Chiron, J. C. & Barnolas, A. (eds) *SynthÈse géologique et géophysique des Pyrénées. Volume 1, Le cycle hercynien*. Orléans: Bureau de Recherches Géologiques et MiniÈres.

Hall, A. (1966*a*). A petrogenetic study of the Rosses granite complex, Donegal. *Journal of Petrology* **7**, 202–220.

Hall, A. (1966*b*). The Ardara pluton: a study of the chemistry and crystallisation of a contaminated granite intrusion. *Proceedings of the Royal Irish Academy* **65B**, 203–235.

Hamilton, W. & Myers, W. B. (1967). The nature of batholiths. *US Geological Survey, Professional Paper* **554-C**, 1–30.

Hildreth, W. (1981). Gradients in silicic magma chambers: implications for lithospheric magmatism. *Journal of Geophysical Research* **86**, 10153–10192.

Holdaway, M. J. (1971). Stability of andalusite and the aluminium silicate phase diagrams. *American Journal of Science* **271**, 97–131.

Holloway, J. R. & Burnham, C. W. (1972). Melting relations of basalt with equilibrium water pressure less than total pressure. *Journal of Petrology* **13**, 1–29.

Huppert, H. E. & Sparks, R. S. J. (1988). The generation of granitic magmas by intrusion of basalt into continental crust. *Journal of Petrology* **29**, 599–624.

Innocent, C., Briqueu, L. & Cabanis, B. (1994). Sr–Nd isotope and trace-element geochemistry of late Variscan volcanism in the Pyrenees: magmatism in post-orogenic extension? *Tectonophysics* **238**, 161–181.

Jacobsen, S. B. & Wasserburg, G. J. (1980). Sm–Nd isotopic evolution of chondrites. *Earth and Planetary Science Letters* **50**, 139–155.

Johannes, W. & Holtz, F. (1996). *Petrogenesis and Experimental Petrology of Granitic Rocks*. Berlin: Springer, 335 pp.

Johnston, A. D. & Wyllie, P. J. (1988). Constraints on the origin of Archean trondhjemites based on phase relationships of Nûk gneiss with $PH_2O$ at 15 kbar. *Contributions to Mineralogy and Petrology* **100**, 35–46.

Kerrick, D. M. (1972). Experimental determination of muscovite + quartz stability with $PH_2O < P_{total}$. *American Journal of Science* **272**, 946–958.

Kretz, R. (1983). Symbols for rock-forming minerals. *American Mineralogist* **68**, 277–279.

Krogh, T. E. (1973). A low-contamination method for hydrothermal decomposition of zircon and extraction of U and Pb for isotopic age determinations. *Geochimica et Cosmochimica Acta* **37**, 485–494.

Krogh, T. E. (1982). Improved accuracy of U–Pb zircon ages by the creation of more concordant systems using an air abrasion technique. *Geochimica et Cosmochimica Acta* **46**, 637–649.

Leake, B. E. (1974). The crystallisation and emplacement of the western part of the Galway granite, Connemara, western Ireland. *Mineralogical Magazine* **39**, 498–513.

Leake, B. E. (1978). Nomenclature of amphiboles. *American Mineralogist* **63**, 1023–1052.

Leterrier, J. (1972). Étude pétrographique et géochimique du massif granitique de Quérigut (AriÈge). ThÈse Doctorat d'État, Université de Nancy, 320 pp.

Leterrier, J. & Debon, F. (1978). CaractÈres chimique comparés des roches granitoides et de leurs enclaves microgrenues. Implications génétiques. *Bulletin de la Societé Géologique de France* **20**, 3–10.

Ludwig, K. R. (1993). Pbdat: a computer program for processing Pb–U–Th isotope data, version 1·24. *US Geological Survey, Open-File Report* **88-542**, 32 pp.

Ludwig, K. R. (1994). Isoplot: a plotting and regression program for radiogenic isotope data, version 2·71. *US Geological Survey, Open-File Report* **91-445**, 44 pp.

Majoor, F. J. M. (1988). A geochronological study of the Axial Zone of the Central Pyrenees, with emphasis on Variscan events and Alpine resetting. Ph.D. Thesis, University of Utrecht, 117 pp.

Marre, J. (1970). Relations texturales et structurales entre les principaux types de roches dans le massif de Quérigut (AriÈge). *Comptes Rendus de l'Académie des Sciences* **271**, 1661–1664.

Marre, J. (1973). Le complex éruptif de Quérigut, pétrologie, structurologie, cinématique de mise en place. ThÈse Doctorat d'État, Université Paul Sabatier, Toulouse, 536 pp.

Matte, P. (1986). Tectonics and a plate tectonics model for the Variscan Belt of Europe. *Tectonophysics* **126**, 329–374.

Matte, P. & Mattauer, M. (1987). Hercynian orogeny in the Pyrenees was not a rifting event. *Nature* **325**, 739–740.

Mattinson, J. M. (1987). U–Pb ages of zircons; a basic examination of error propagation. *Chemical Geology* **66**, 151–162.

McCaig, A. M. & Miller, J. A. (1986). $^{40}Ar$–$^{39}Ar$ age of mylonites along the Merens Fault, central Pyrenees. *Tectonophysics* **129**, 149–172.

Michard-Vitrac, A., AlbarÈde, F., Dupuis, C. & Taylor, H. P. (1980). The genesis of Variscan (Hercynian) plutonic rocks: inferences from Sr, Pb, and O studies on the Maladeta Igneous Complex, Central Pyrenees (Spain). *Contributions to Mineralogy and Petrology* **72**, 57–72.

Mogessie, A., Tessadri, R. & Veltman, C. B. (1990). EMP-AMPH; a Hypercard program to determine the name of an amphibole from electron microprobe analysis according to the International Mineralogical Association scheme. *Computers and Geosciences* **16**, 309–330.

Nakada, S. (1983). Zoned magma chamber of the Osuzuyama acid rocks, south-west Japan. *Journal of Petrology* **24**, 471–494.

Naney, M. T. (1983). Phase equilibria of rock forming ferromagnesian silicates in granitic systems. *American Journal of Science* **283**, 993–1033.

Ortoleva, P. J. (1994). *Geochemical Self-Organization*. Oxford: Oxford University Press, 411 pp.

Paquette, J. L., Gleizes, G., Leblanc, D. & Bouchez, J. L. (1997). Le granite de Bassiés (Pyrénées): un pluton syntectonique d'âge Westphalien. Géochronologie U–Pb sur zircons. *Comptes Rendus de l'Académie des Sciences* **324**, 387–392.

Parrish, R. L. (1987). An improved micro-capsule for zircon dissolution in U–Pb geochronology. *Chemical Geology* **66**, 99–102.

Peccerillo, A. & Taylor, S. R. (1976). Geochemistry of Eocene calc-alkaline volcanic rocks from the Kastamonu area, northern Turkey. *Contributions to Mineralogy and Petrology* **58**, 63–81.

Pin, C. (1989). Essai sur la chronologie et l'évolution géodynamique de la chaîne Hercynienne d'Europe. ThÈse Doctorat d'État, Université Blaise Pascal, Clermont-Ferrand, 470 pp.

Pin, C. (1990). Evolution of the lower crust in the Ivrea Zone: a model based on isotopic and geochemical data. In: Vielzeuf, D. & Vidal, P. (eds) *Granulites and Crustal Differentiation*. Dordrecht: Kluwer Academic, pp. 87–110.

Pitcher, W. S. (1987). Granites and yet more granites forty years on. *Geologische Rundschau* **76**, 51–79.

Piwinskii, A. J. (1968). Experimental studies of igneous rock series, central Sierra Nevada Batholith, California. *Journal of Geology* **76**, 548–570.

Pons, J. (1970). Relations entre la structure est la pétrofabrique des roches éruptives dans la bordure méridonale du massif granitique de Quérigut (AriÈge). *Comptes Rendus de l'Académie des Sciences* **271**, 1665–1668.

Presnall, D. C. & Bateman, P. C. (1973). Fusion relations in the system $NaAlSi_3O_8$–$CaAl_2Si_2O_8$–$KAlSi_3O_8$–$SiO_2$–$H_2O$ and the generation of granitic magmas in the Sierra Nevada Batholith. *Geological Society of America Bulletin* **84**, 3181–3202.

Provost, A. (1990). An improved diagram for isochron data. *Chemical Geology* **80**, 85–99.

Pupin, J. P. (1980). Zircon and granite petrology. *Contributions to Mineralogy and Petrology* **73**, 207–220.

Raymond, D. & Marre, J. (1988). Les septa métasédimentaires du pluton granitique de Quérigut (Est des Pyrénées, France), reliques d'une unité allochtone varisque. *Comptes Rendus de l'Académie des Sciences, Série 2*, **307**, 1107–1112.

Roberts, M. P. (1994). Petrogenetic relationships between gabbros, diorites, ultramafic rocks, granites and their enclaves, Quérigut Massif, French Pyrenees. Ph.D. Thesis, University of Manchester, 361 pp.

Roberts, M. P. & Clemens, J. D. (1993). Origin of high potassium, calc-alkaline, I-type granitoids. *Geology* **21**, 825–828.

Roberts, M. P. & Clemens, J. D. (1994). Low-pressure stability of magmatic epidote in granitoid plutons: field and experimental evidence. Volcanic Studies Group 4th Annual Thematic and Research in Progress Meeting Abstracts. Liverpool: University of Liverpool, p. 30.

Roberts, M. P. & Clemens, J. D. (1995). Feasibility of AFC models for the petrogenesis of calc-alkaline magma series. *Contributions to Mineralogy and Petrology* **121**, 139–147.

Roberts, M. P. & Clemens, J. D. (1997). Correction to 'Feasibility of AFC models for the petrogenesis of calc-alkaline magma series'. *Contributions to Mineralogy and Petrology* **128**, 97–99.

Robertson, J. K. & Wyllie, P. J. (1971). Rock–water systems with special reference to the water-deficient region. *American Journal of Science* **271**, 252–277.

Rollinson, H. R. (1993). *Using Geochemical Data: Evaluation, Presentation, Interpretation*. Harlow: Longman, 352 pp.

Romer, R. L. & Soler, A. (1995). U–Pb age and lead isotopic characterization of Au-bearing skarn related to the Andorra granite (central Pyrenees, Spain). *Mineralium Deposita* **30**, 374–383.

Sandiford, M. & Powell, R. (1986). Deep crustal metamorphism during continental extension: modern and ancient examples. *Earth and Planetary Science Letters* **79**, 151–158.

Sawka, W. N., Chappell, B. W. & Kistler, R. W. (1990). Granitoid compositional zoning by side-wall boundary layer differentiation: evidence from the Palisade Crest intrusive suite, central Sierra Nevada, California. *Journal of Petrology* **31**, 519–553.

Schmidt, M. W. & Thompson, A. B. (1996). Epidote in calc-alkaline magmas: an experimental study of stability, phase relationships, and the role of epidote in magma evolution. *American Mineralogist* **81**, 462–474.

Shand, S. J. (1947). *Eruptive Rocks. Their Genesis, Composition, Classification, and their Relation to Ore-Deposits*. New York: John Wiley.

Shaw, H. R. (1965). Comments on viscosity, crystal settling, and convection in granitic magmas. *American Journal of Science* **263**, 120–152.

Silver, L. T. & Chappell, B. W. (1988). The Peninsular Ranges Batholith: an insight into the evolution of the Cordilleran batholiths of southwestern North America. *Philosophical Transactions of the Royal Society, Edinburgh* **79**, 105–121.

Soula, J. C., Lamouroux, C., Viallard, P., BessiÈre, G., Debat, P. & Ferret, B. (1986). The mylonite zones in the Pyrenees and their place in the Alpine tectonic evolution. *Tectonophysics* **129**, 115–147.

Stacey, J. S. & Kramers, J. D. (1975). Approximation of the terrestrial lead isotope evolution by a two-stage model. *Earth and Planetary Science Letters* **26**, 207–221.

Steiger, R. H. & Jäger, E. (1977). Subcommission on geochronology: convention on the use of decay constants in geo- and cosmochronology. *Earth and Planetary Science Letters* **36**, 359–362.

Taylor, W. P. (1976). Intrusion and differentiation of granitic magma at a high level in the crust: the Puscao pluton, Lima Province, Peru. *Journal of Petrology* **17**, 194–218.

Tepper, J. H., Nelson, B. K., Bergantz, G. W. & Irving, A. J. (1993). Petrology of the Chilliwack batholith, North Cascades, Washington: generation of calc-alkaline granitoids by melting of mafic lower crust with variable water fugacity. *Contributions to Mineralogy and Petrology* **113**, 333–351.

Tracy, R. J. & Frost, B. R. (1991). Phase equilibria and thermobarometry of calcareous, ultramafic and mafic rocks, and iron formations. In: Kerrick, D. M. (ed.) *Contact Metamorphism. Mineralogical Society of America, Reviews in Mineralogy* **26**, 207–290.

Tuttle, O. F. & Bowen, N. L. (1958). Origin of granite in the light of experimental studies in the system $NaAlSi_3O_8$–$KAlSi_3O_8$–$SiO_2$–$H_2O$. *Geological Society of America, Memoir* **74**, 153 pp.

Vance, J. A. (1962). Zoning in igneous plagioclase: normal and oscillatory zoning. *American Journal of Science* **260**, 746–760.

Van den Eeckhout, B. & Zwart, H. J. (1988). Hercynian crustal-scale extensional shear zone in the Pyrenees. *Geology* **16**, 135–138.

Vernon, R. H. (1986). K-feldspar megacrysts in granites—phenocrysts not porphyroblasts. *Earth-Science Reviews* **23**, 1–63.

Vielzeuf, D. (1980). Pétrologie des écailles granulitiques de le région de Lherz (AriÈge–Zone Nord Pyrénéene). Introduction à l'étude expérimental de l'association grenat (Alm–Pyr)–feldspath potassique. 3rd Cycle Thesis, Université Blaise Pascal, Clermont-Ferrand, 219 pp.

Vielzeuf, D. (1984). Rélations de phases dans le faciÈs granulite et implications géodynamiques. L'exemple des granulites des Pyrénées. Ph.D. Thesis, Université Blaise Pascal, Clermont-Ferrand, 288 pp.

Vielzeuf, D., Clemens, J. D., Pin, C. & Moinet, E. (1990). Granites, granulites and crustal differentiation. In: Vielzeuf, D. & Vidal, P. (eds) *Granulites and Crustal Differentiation*. Dordrecht: Kluwer Academic, pp. 59–86.

Vissers, R. L. M. (1992). Variscan extension in the Pyrenees. *Tectonics* **11**, 1369–1384.

Vitrac-Michard, A. & Allègre, C. J. (1975). A study of the formation and history of a piece of continental crust by Rb–Sr method: the case of the French oriental Pyrenees. *Contributions to Mineralogy and Petrology* **50**, 257–285.

Wall, V. J., Clemens, J. D. & Clarke, D. B. (1987). Models for granitoid evolution and source compositions. *Journal of Geology* **95**, 731–749.

Wasserburg, G. J., Jacobsen, S. B., DePaolo, D. J., McCulloch, M. T. & Wen, T. (1981). Precise determination of Sm/Nd ratios, Sm and Nd isotopic abundances in standard solutions. *Geochimica et Cosmochimica Acta* **45**, 2311–2323.

Weber, K. & Behr, H.-J. (1983). Geodynamic interpretation of the mid-European Variscides. In: Martin, H. & Eder, F. W. (eds) *Intracontinental Fold Belts*. Berlin: Springer, pp. 427–469.

White, A. J. R. & Chappell, B. W. (1977). Ultrametamorphism and granitoid genesis. *Tectonophysics* **43**, 7–22.

Wickham, S. M. & Oxburgh, E. R. (1985). Continental rifts as a setting for regional metamorphism. *Nature* **318**, 330–333.

Wickham, S. M. & Oxburgh, E. R. (1987). Low pressure regional metamorphism in the Pyrenees and its implications for the thermal evolution of rifted continental crust. *Philosophical Transactions of the Royal Society of London, Series A* **321**, 219–243.

Williams, G. H. (1886). Art. 4—The peridotites of the 'Cortlandt series' on the Hudson River near Peekshill, New York. *American Journal of Science* **31**, 26–41.

Wyborn, D. & Chappell, B. W. (1986). The petrogenetic significance of chemically related plutonic and volcanic rock units. *Geological Magazine* **6**, 619–628.

Wyllie, P. J. (1977). Crustal anatexis: an experimental overview. *Tectonophysics* **43**, 41–71.

Zen, E.-A. & Hammarstrom, J. M. (1984). Magmatic epidote and its petrologic significance. *Geology* **12**, 515–518.

Zwart, H. J. (1986). The Variscan geology of the Pyrenees. *Tectonophysics* **129**, 9–27.

# APPENDIX A: ANALYTICAL TECHNIQUES

## Whole-rock major and trace element analysis

Whole-rock major element and trace element analyses were performed by X-ray fluorescence spectrometry using a Phillips PW1450 spectrometer at Manchester University, on 30 mm diameter, boric acid-backed, pressed-powder pellets. Techniques for data treatment and correction have been given by Brown *et al.* (1973). Instrumental conditions and analytical errors have been given by Roberts (1994).

## Mineral analysis

Mineral analysis was performed using a Cambridge Instruments Geoscan electron probe micro-analyser, with a Link Systems QX 2000 energy-dispersive analysis system combined with ZAF4–FLS deconvolution–recalculation package at Manchester University. A focused beam and accelerating voltage of 15 kV were used over a live time of 40 s per analysis. The average detection limit is 0·1% at $2\sigma$ confidence limit.

## Isotopic analysis

All isotope analyses were performed at the CNRS, Clermont-Ferrand. HF, HCl and $HNO_3$ used in sample preparation were analytical grade reagents (Prolabo), distilled in silica glass stills (Quartex, Paris) or sub-boiling PFA Teflon stills. $H_2O$ was purified through a Milli-Q system (Millipore). Blank analyses were in the region of 5 pg for Pb, 0·5 pg for U, 1 ng for Rb and Sr, and 0·1 ng for Sm and Nd.

## U–Pb zircon analysis

Non-magnetic zircon crystals, with a minimum of imperfections, were hand picked and mechanically abraded (Krogh, 1982). Zircon dissolution and chemical separation of U and Pb were carried out according to Krogh (1973) and Parrish (1987), with modifications described by Paquette *et al.* (1997). Pb analyses were corrected for a blank isotopic composition of $^{206}Pb/^{204}Pb = 18{\cdot}1$, $^{207}Pb/^{204}Pb = 15{\cdot}6$ and $^{208}Pb/^{204}Pb = 38{\cdot}0$. The U and Pb isotopes were analysed on a Fisons VG Sector 54-30 mass spectrometer in multi-collector static mode. The $^{204}Pb$ was simultaneously measured with a Daly detector ion counting system. Repeated measurement of the NBS

982 standard yielded a mass fractionation correction factor of 0·1% per a.m.u. Pb and U were loaded with silica gel and $H_3PO_4$ on the same single Re filament and run subsequently at 1500–1600°C for Pb and >1600°C for $UO_2$. The raw data were treated using the normalization values and decay constants recommended by Steiger & Jäger (1977). Data errors ($2\sigma$) of the zircon fractions and discordia lines were calculated using the PBDAT 1·24 and ISOPLOT 2·71 programs (Ludwig, 1993, 1994).

### Whole-rock Rb–Sr isotopic analysis

Approximately 0·1 g of each sample was weighed accurately into PFA Teflon vials (Savillex, Minnetonka, USA) and spiked with a mixed $^{84}Sr$–$^{87}Rb$ tracer. Rb and Sr were separated using Bio-Rad ion-exchange resin AG50 × 8 (200–400 mesh) in 2·5 M HCl. For samples with high Rb/Sr ratios a further step was performed to eliminate isobaric interference of $^{87}Rb$ with $^{87}Sr$. For this, the Sr-bearing fraction was loaded onto 1 ml columns containing AG50 × 12 ion-exchange resin and eluted with 2·7 M HCl. The Rb-bearing fraction was loaded onto small columns containing 0·5 ml PHOZIR (zirconium phosphate) and recovered in 2·5 ml of a mixture of 2 M $NH_4Cl$ and 2 M HCl. $NH_4Cl$ was decomposed by the addition of 1·5 ml of concentrated $HNO_3$ and heating for 36 h under an IR lamp. Sr was dissolved in a single drop of deionized water, and 1–3 μg Sr loaded onto flat, degassed Ta single filaments in 3 M $H_3PO_4$. Rb was dissolved in three drops of deionized water and loaded onto flat, degassed Ta single filaments in 1 M $H_3PO_4$.

Rb concentrations were measured using a single-collector Cameca TSN 206 mass spectrometer. Sr isotope analysis was performed with a fully automated VG ISOMASS 54E mass spectrometer in double collection mode. For this, 50–100 averaged blocks of 10 measurements were taken at a total ion beam current of 40 pA. Automatic termination of each analysis occurred when the relative $^{87}Sr/^{86}Sr$ precision reached $\pm 0{\cdot}00003$ ($2\sigma$).

### Whole-rock Sm–Nd isotopic analysis

Approximately 0·1 g of each sample was accurately weighed into Teflon-lined stainless steel digestion vessels, and spiked with $^{150}Nd$–$^{149}Sm$ mixed tracer solution. The light rare earth elements (LREE) and heavy REE (HREE) were separated using TRU-SPEC. SPS resin (EIChroM Industries, Darien, IL, USA). The HREE were removed with 2 M $HNO_3$ and the Sm- and Nd-bearing LREE fraction was eluted with 0·05 M $HNO_3$.

Separation of Sm from Nd and from the other LREE was carried out using DEP (diethyl-hexyl-phosphoric acid) adsorbed onto an inert support. Elution of La, Ce and Pr was achieved using 0·25 M HCl. Nd was collected in 0·3 M HCl, and Sm was eluted with 0·67 M HCl. Sm was loaded onto flat, degassed Ta single filaments in 3 M $H_3PO_4$, and Nd onto one of the Ta side filaments of Ta–Re–Ta triple filament assemblies, in 1 M $H_3PO_4$. The isotopic analyses were performed with a fully automated VG ISOMASS 54E mass spectrometer in double collection mode. For this, 50–100 averaged blocks of 10 measurements were taken at a total ion beam current of 20–40 pA.

## APPENDIX B: SAMPLE LOCALITIES

The grid references quoted are those of the Mercator universal system on the French 1:25 000 scale topographic maps [Sheets 2348 ouest (Axat), 2249 ET (Font Romeu), 2248 est (Quérigut) and 2448 ET (Ille-sur-Têt)]. Locality names refer to the nearest geographical feature marked on the topographic map.

| Sample | Description | Locality |
|---|---|---|
| *Granodiorites and tonalites* | | |
| QH29 | Bt tonalite | near Étang de Laurenti 4215/47264 |
| QH56 | foliated granodiorite | Pic de Baxouillade 4182/47239 |
| QH70 | altered Bt tonalite | Campeilles 4244/47262 |
| QH76 | granodiorite | Roc de Fronteils 4208/47258 |
| QH107 | Bt tonalite | Prat Baillet 4261/47249 |
| QH146 | Bt tonalite | near former Fe mine of Boutadiol 4207/47247 |
| QH170 | foliated Bt tonalite | Coume de Barbouillère 4186/47256 |
| QH179 | foliated granodiorite | south of Jasse de Peyron 4239/47234 |
| QH214 | Bt tonalite | Étang de Laurenti 4200/47252 |
| QH217 | Bt tonalite | Roc de Fronteils 4208/47258 |
| QZ233 | Hbl Bt tonalite | Quarry near Puyvalador 4284/47237 |
| *Monzogranites* | | |
| QH13 | Or-phyric monzogranite | la Rouquette 4288/47238 |
| QH34 | Mc-phyric monzogranite | la Calhau Jace 4380/47245 |

| Sample | Description | Locality |
|---|---|---|
| QH45 | Or-phyric monzogranite | Tuc de Cantolèbres 4331/47310 |
| QH53 | Mc-phyric monzogranite | Pic de Coumeille de l'Ours 4164/47294 |
| QH126 | Kfs-phyric monzogranite | Bains de Carcanières 4281/47302 |
| QH130 | Kfs-phyric monzogranite | D118 below Serrat de Puch 4292/47297 |
| QH133 | Mc-phyric monzogranite | Jasse d'Enclot 4296/47254 |
| QH148 | Mc-phyric monzogranite | Campeil 4208/47297 |
| QH239 | Or-bearing aphyric monzogranite | la Forge 4355/47319 |
| QH241 | Mc-phyric monzogranite | near Col de Jau 4388/47259 |
| *Biotite granite* | | |
| QH89 | Or-bearing Bt granite | Col de Carcanières 4270/47292 |
| QH127 | Or-bearing Bt granite | Bains de Carcanières 4282/47301 |
| *Diorites* | | |
| QM50 | Pl phyric Hbl–Bt diorite | Quarry near Puyvalador 4284/47237 |
| QM109 | Hbl-phyric diorite | Pujol d'en Tartra 4262/47252 |
| QM138 | Pl-phyric diorite | Bois de Jacoumet 4294/47259 |
| QM197 | Bt-phyric diorite | Étang de la Camisette 4186/47261 |
| QM213 | Pl-phyric Hbl–Bt diorite | Étang de Laurenti 4200/47252 |
| QM228 | Pl-phyric diorite | Bois de Limouse 4257/47262 |
| QM236 | Pl-phyric diorite | les Casalets 4285/47239 |
| *Hornblende gabbros* | | |
| QM77 | Hbl gabbro | near former Fe mine of Boutadiol 4207/47247 |
| QM119 | Hbl gabbro | la Restanque 4181/47281 |
| QM144 | Hbl gabbro | near former Fe mine of Boutadiol 4207/47247 |
| *Ultramafic rocks* | | |
| QUM5 | hornblendite | Bousadus de Bas 4213/47279 |
| QUM6 | Ol Phl hornblendite | Bousadus de Bas 4213/47279 |
| QUM7(1) | Ol Phl hornblendite | Bousadus de Bas 4213/47279 |
| QUM8 | altered Ol Phl hornblendite | Bousadus de Bas 4213/47279 |
| QUM64 | altered Ol Phl hornblendite | Roc de Campeilles 4245/47264 |
| QUM68 | hornblendite | Campeilles 4244/47262 |
| QUM71 | Ol Phl hornblendite | la Restanque 4181/47281 |
| QUM226 | Pl-bearing Ol Phl hornblendite | 4198/47270 |